NAVAL POSTGRADUATE SCHOOL
MONTEREY, CALIFORNIA

THESIS

THERMAL BOUNDARY RESISTANCE IN A HIGH TEMPERATURE THIN-FILM SUPERCONDUCTOR UNDER VARYING HEAT FLUX

by

Michael P. Magee

December, 1996

Thesis Advisor: Matthew D. Kelleher
Co-Advisor: Patrick E. Phelan (ASU)

Approved for public release; distribution is unlimited.

REPORT DOCUMENTATION PAGE

Form Approved OMB No. 0704-

1. AGENCY USE ONLY *(Leave blank)*	2. REPORT DATE December 1996	3. REPORT TYPE AND DATES COVERED Master's Thesis

4. TITLE AND SUBTITLE: THERMAL BOUNDARY RESISTANCE IN A HIGH TEMPERATURE THIN-FILM SUPERCONDUCTOR UNDER VARYING HEAT FLUX

5. FUNDING NUMBERS

6. AUTHOR(S) Michael P. Magee

7. PERFORMING ORGANIZATION NAME(S) AND ADDRESS(ES)
Naval Postgraduate School
Monterey, CA 93943-5000

8. PERFORMING ORGANIZATION REPORT NUMBER

9. SPONSORING/MONITORING AGENCY NAME(S) AND ADDRESS(ES)

10. SPONSORING/MONITORING AGENCY REPORT NUMBER

11. SUPPLEMENTARY NOTES The views expressed in this thesis are those of the author and do not reflect the official policy or position of the Department of Defense or the U.S. Government.

12a. DISTRIBUTION/AVAILABILITY STATEMENT
Approved for public release; distribution is unlimited.

12b. DISTRIBUTION CODE

13. ABSTRACT *(maximum 200 words)*

The thermal boundary resistance between a $YBa_2Cu_3O_7$ thin-film and an MgO substrate was measured under conditions of varying heat flux. Heat flux was varied in a manner to explore any hysteresis effects present. It was concluded that hysteresis effects are present and are most likely attributed to changes in the peeling or compressive stresses in the thin-film. The changes in the peeling stresses may not be fully relieved after cycling of the heat flux or may have caused microstructural changes near the interface resulting in changes in microscale heat transfer characteristics. Additionally, finite difference method were used to model the physical situation. It was found that boundary resistance values generated by the computer program were several orders of magnitude less than experimental value. It was concluded that finer meshes must be used in order to increase the accuracy of the results. It was recommended that the modeling be redone on a main frame computer using finite element methods.

14. SUBJECT TERMS SUPERCONDUCTORS, THIN-FILMS, THERMAL BOUNDARY RESISTANCE, HEAT FLUX, HYSTERESIS

15. NUMBER OF PAGES 88

16. PRICE CODE

17. SECURITY CLASSIFICATION OF REPORT	18. SECURITY CLASSIFICATION OF THIS PAGE	19. SECURITY CLASSIFICATION OF ABSTRACT	20. LIMITATION OF ABSTRACT
Unclassified	Unclassified	Unclassified	UL

NSN 7540-01-280-5500

Standard Form 298 (Rev. 2-89)
Prescribed by ANSI Std. 239-18 298-102

Approved for public release; distribution is unlimited.

THERMAL BOUNDARY RESISTANCE IN A HIGH TEMPERATURE THIN-FILM SUPERCONDUCTOR UNDER VARYING HEAT FLUX

Michael P. Magee
Lieutenant, United States Navy
B.S.M.E., Auburn University, 1987

Submitted in partial fulfillment
of the requirements for the degree of

MASTER OF SCIENCE IN MECHANICAL ENGINEERING

from the

NAVAL POSTGRADUATE SCHOOL
December 1996

Author: _____
Michael P. Magee

Approved by: _____
Matthew D. Kelleher, Thesis Advisor

_____
Patrick E. Phelan, Co-Advisor

_____
Terry R. McNelley, Chairman
Department of Mechanical Engineering

ABSTRACT

The thermal boundary resistance between a $YBa_2Cu_3O_7$ thin-film and an MgO substrate was measured under conditions of varying heat flux. Heat flux was varied in a manner to explore any hysteresis effects present. It was concluded that hysteresis effects are present and are most likely attributed to changes in the peeling or compressive stresses in the thin-film. The changes in the peeling stresses may not be fully relieved after cycling of the heat flux or may have caused microstructural changes near the interface resulting in changes in microscale heat transfer characteristics. Additionally, finite difference method were used to model the physical situation. It was found that boundary resistance values generated by the computer program were several orders of magnitude less than experimental value. It was concluded that finer meshes must be used in order to increase the accuracy of the results. It was recommended that the modeling be redone on a main frame computer using finite element methods.

TABLE OF CONTENTS

I. INTRODUCTION 1

II. BACKGROUND 3

A. THERMAL BOUNDARY RESISTANCE 3

1. Heat Transfer 3

2. Characterization of R_b 5

3. Mathematical Modeling 7

B. YBCO THIN-FILM SUPERCONDUCTORS 9

1. YBCO 9

2. Thermal Properties 9

III. EXPERIMENTAL 15

A. MATERIALS 15

B. EQUIPMENT 19

C. PROCEDURE 22

IV. RESULTS AND DISCUSSION 27

A. R_b CORRECTIONS 27

B. UNCERTAINTY ANALYSIS 30

1. Uncertainty Equation 30

2. Temperature Difference Uncertainty . . . 32

3. Heat Flux Uncertainty 33

4. Radiation Loss Uncertainty 39

5. Uncertainty in R_b 40

C. R_b VARIATION WITH HEAT FLUX 42

D. HYSTERESIS EFFECTS 44

E. FINITE DIFFERENCE METHODS 49

V. RECOMMENDATIONS 57

APPENDIX A. SUBSTRATE TEMPERATURE DISTRIBUTION 59

APPENDIX B. FINITE DIFFERENCE PROGRAM 67

LIST OF REFERENCES 73

INITIAL DISTRIBUTION LIST 77

ACKNOWLEDGEMENTS

The author would like to acknowledge the financial support of the National Science Foundation for providing research funds under grant number CTS-969002.

Appreciation is extended to Professor Matthew D. Kelleher for his guidance and oversight which allowed this thesis to be completed. The author acknowledges Professor Patrick E. Phelan whose expertise and fascination with the field of high-temperature superconductors made this project possible.

Appreciation is extended to my partners Mukul Kelkar and Bei Gu who provided the corporate knowledge in the operation of the experimental setup which allowed us to overcome many obstacles in the data acquisition process. Woo-Wai Lau is acknowledged for her superb etching skills which brought the required film patterns to life.

Finally, deepest appreciation is extended to Pam Davis who handled the administrative matters required to complete this thesis. Equally important, though, was the moral support provided by Pam during the thesis process which was instrumental in sustaining the author's determination to finish.

I. INTRODUCTION

The thermal boundary resistance between a superconducting film and the substrate can strongly affect the thermal design of devices made from high-temperature superconductors (HTS). Heat dissipation has always been an important factor in the design of electronic devices. In thin-film HTS devices, poor heat transfer may result in the device being driven from the superconducting to the normal state. In a superconductivity application this would prevent the device from functioning as designed.

The current use of superconducting electronic devices falls into two basic classes: SQUID systems, which are used to directly measure magnetic flux; and Josephson devices, which perform traditional electronic functions [Ref. 1]. The thermal stability of thin films is crucial due to their critical temperature requirements and small size, and is highly dependent upon the thermal boundary resistance (R_b) between the film and the substrate [Ref. 2]. While some characterization of R_b has been done, including the effects of heat flux, further investigation is warranted [Ref. 2,3]. In particular, no study has been done to date on the hysteresis effects on R_b resulting from varying the heat flux.

Accordingly, the goal of this study is to vary the heat flux applied to a $YBa_2Cu_3O_7$ thin film on a MgO substrate in the normal state and investigate the effects on R_b. Heat flux will be varied at several different substrate temperatures and will be cycled to observe any hysteresis effects.

Additionally, efforts will be made to use finite difference numerical techniques to model the physical situation. Current experimental techniques do not allow the measurement of the temperature in the substrate directly below the thin-film; this temperature must be solved for using the Laplace equation. Finite difference modeling will yield a temperature distribution that may allow refinement of experimental values for increased R_b accuracy.

II. BACKGROUND

A. THERMAL BOUNDARY RESISTANCE

1. Heat Transfer

Whenever there is a contact of two surfaces, a thermal resistance to heat transfer R_b occurs at the interface resulting in a temperature discontinuity. This is illustrated in Figures 1 and 2. It is attributed to imperfect contact, and acoustic and/or lattice mismatch.

The heat transfer across an interface can be considered as a net flow of phonons (and/or electrons) between the two surfaces. The phonon (and/or electron) transmission probabilities can be calculated to determine the heat flux. At low temperatures, R_b is explained by considering an acoustic mismatch between the two solids at the interface. If the acoustic impedances of the two media are very different, then phonon scattering occurs.

An idealized case of a solid-helium interface, thermal boundary resistance is often called the Kapitza resistance, which is explained according to the acoustic mismatch (AMM) theory [Ref. 4]. This theory has been extended to solid-solid boundaries, however, its prediction, except at low temperatures, is lower than empirical values [Ref. 5]. Recently, the AMM theory was modified to include the effects of anharmonic interactions in crystals. Inclusion of

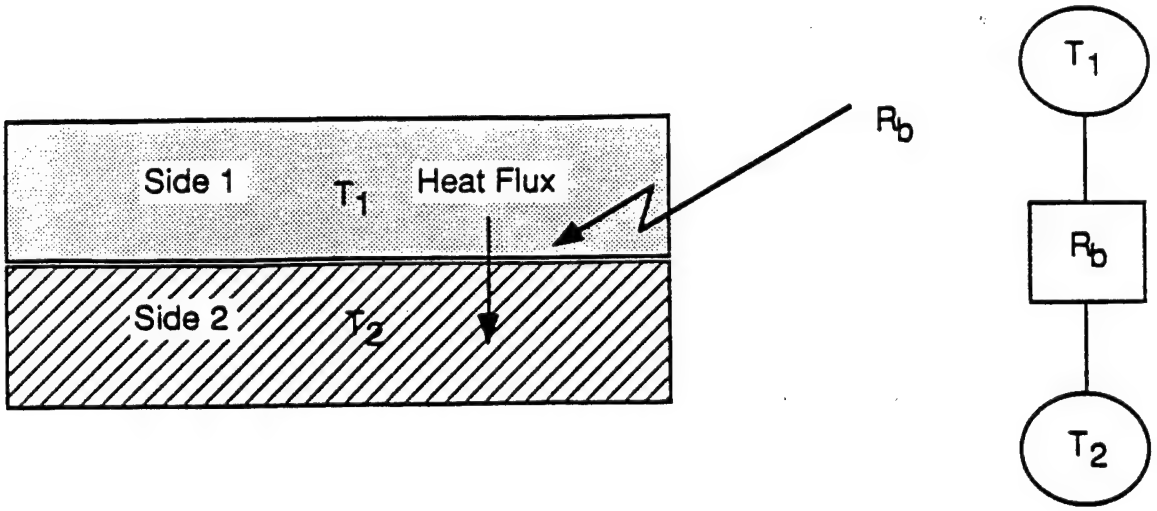

Figure 1. Interface Between Two Surfaces [Ref. 6]

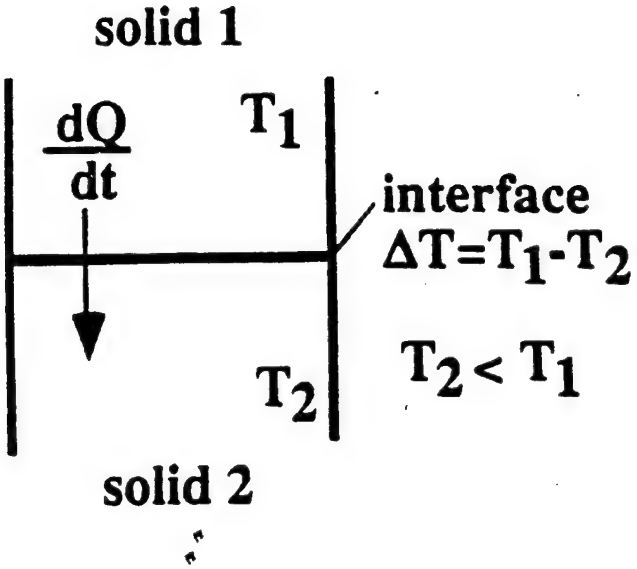

Figure 2. Interface Temperature Discontinuity [Ref. 7]

these Umklapp-processes in the AMM theory (U-AMM) resulted in R_b values that lie closer to experimental data [Ref. 8]. However, the disparity between theoretical and experimental values at temperatures > 30 K still necessitates experimental characterization of R_b.

2. Characterization of R_b

The thermal boundary resistance (R_b) between thin-film HTS and their substrates has been measured. The experimental measurement techniques are fully described in Phelan et al. [Ref. 9] and are based on the methods introduced by Swartz and Pohl [Ref. 10]. Using this technique, previously measured values for R_b for an Er-Ba-Cu-O thin-film on MgO substrate with a T_c of approximately 69 K were found to be on the order of 10^{-3} K-cm^2/W [Ref. 11].

Previous measurements were conducted using two different etching patterns for the film: two parallel strips of equal length in a straight pattern, and two strips of unequal length in a meander pattern (Figures 3 and 4). The straight pattern has the advantage of being simple and, thus, easier to etch. The meander pattern is more complicated, but was designed with a smaller heater/sensor separation than the straight pattern, and was meant to provide more film area for radiative property measurements. Both patterns have only one heater and one sensor strip that, if damaged during fabrication, will render the sample useless.

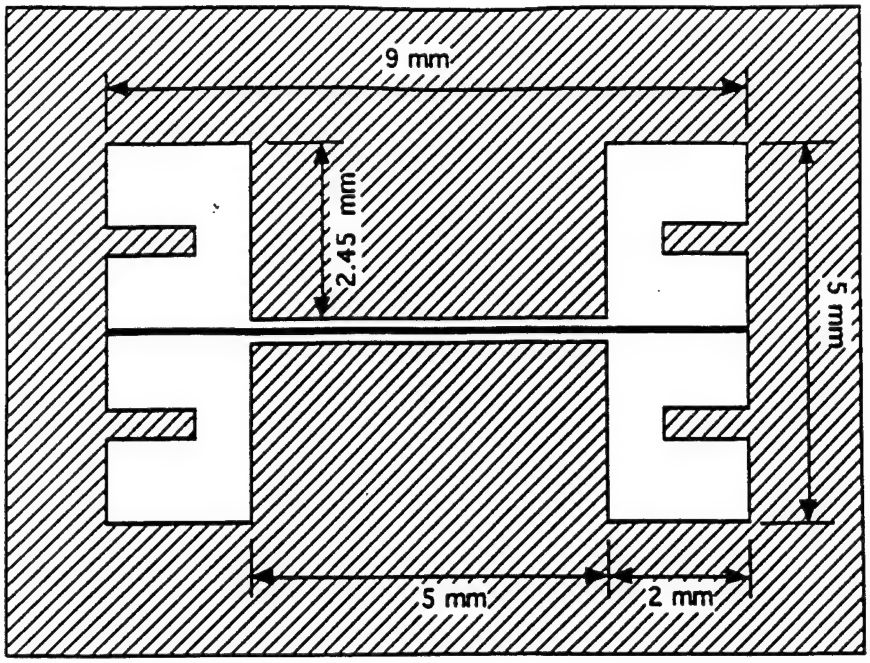

Figure 3. Straight Pattern

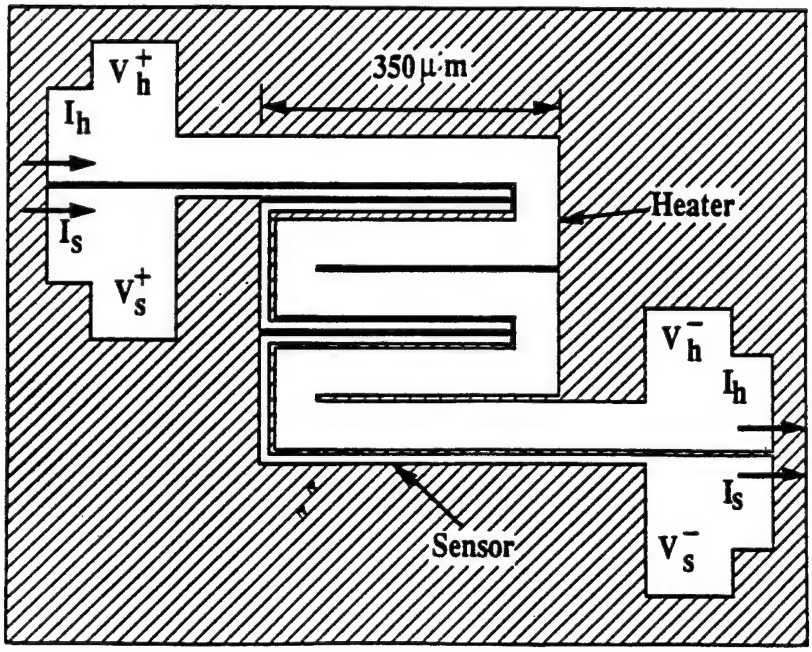

Figure 4. Meander Pattern

The film under test in this study utilized four parallel strips etched in the $YBa_2Cu_3O_7$ thin-film, as shown in Figure 5. Should an etching imperfection occur in one of the strips, other adjacent pairs will be available for use. Both strips are of equal width and either can function as the heater or the sensor. The question remains whether two non-adjacent film strips can be used for data acquisition. The use of the finite difference numerical technique may hold the answer.

3. Mathematical Modeling

The finite difference technique will be used to model the film-substrate response to a temperature or a heat flux imposed on one of the four thin-film strips. The control volume approach will be used to obtain a graded network that can be varied to minimize the overall number of nodes in the network, yet maximize accuracy within the heat affected zone [Ref. 12]. Due to the large number of nodes expected, a Gauss-Seidel algorithm will be used for the program [Ref. 13].

The results of the program will, at the very least, yield a qualitative representation of the temperature distribution within the substrate. The goal is to obtain a value for the temperature of the substrate directly beneath the heater strip. This temperature will be used to bias the experimental results to obtain a more accurate value for R_b.

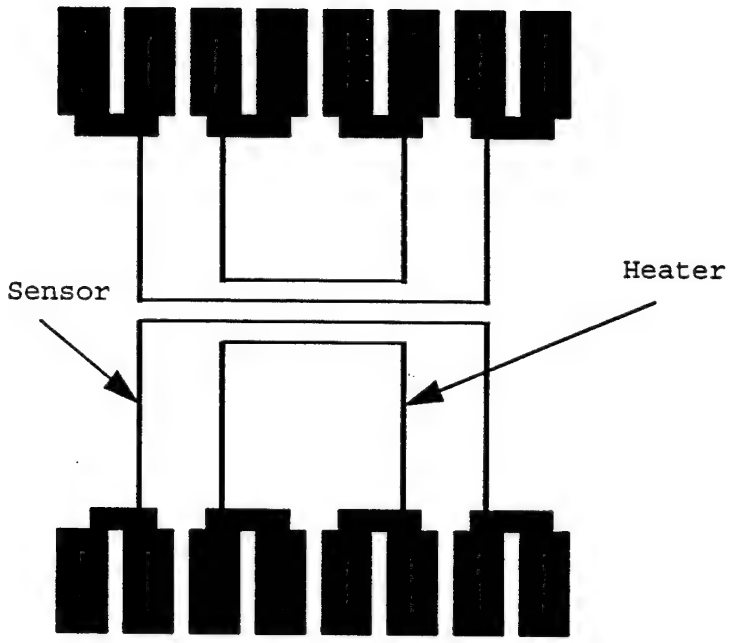

Figure 5. Four Strip Pattern

B. YBCO THIN-FILM SUPERCONDUCTORS

1. YBCO

Sintered samples of $YBa_2Cu_3O_{7-x}$ exhibit superconductivity at temperatures above the boiling point of liquid nitrogen (77 K). The structures of the $YBa_2Cu_3O_7$ unit cell and multicellular $YBa_2Cu_3O_7$ are shown in Figures 6 and 7 respectively. The Cu-O planes are assumed to be the focus of the superconductivity mechanism. The oxygen concentration determines whether the material is superconducting or not. The onset of superconductivity occurs at a value of x=0.55 (7-x=6.45) as the YBCO structure changes from tetragonal (non superconducting) to orthorhombic (superconducting). [Ref. 17]

2. Thermal Properties

The thermal conductivity (k) of $YBa_2Cu_3O_7$ figures prominently in both the error analysis and the finite difference methods used in this study. Given the structure of the unit cell, it is not surprising that the thermal conductivity is anisotropic.

Values of temperature vs thermal conductivity values of YBCO are shown in Figure 8 [Ref. 18]. Thermal conductivity in the c-plane is critical to the heat transfer from the heater strip into the substrate. Thermal conductivity in the ab-plane figures prominently in the error analysis when evaluating for conduction losses in the film lead.

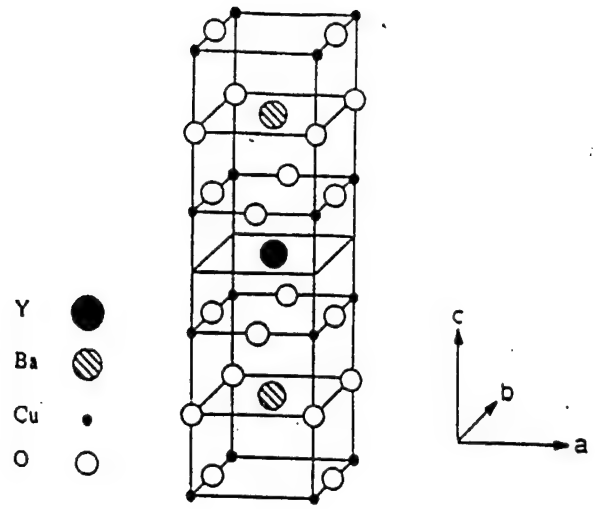

Figure 6. Structure of the $YBa_2Cu_3O_7$ unit cell [Ref. 15]

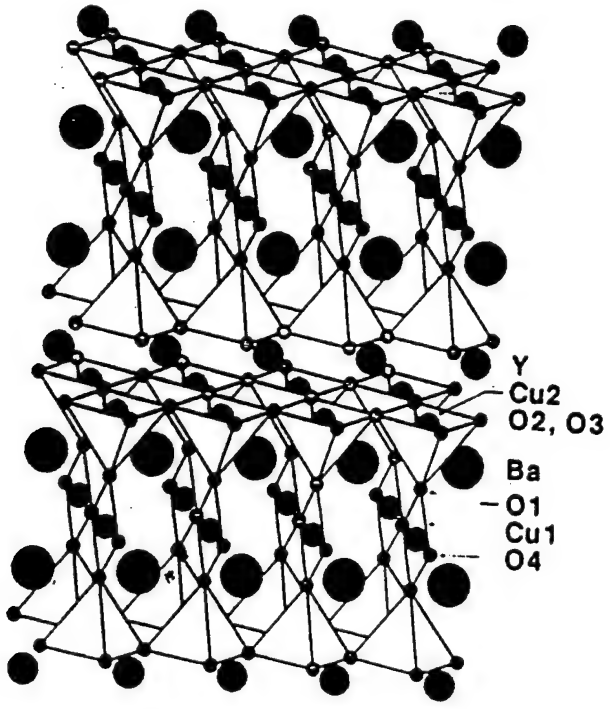

Figure 7. Structure of YBa_2Cu_3O7 [Ref. 16]

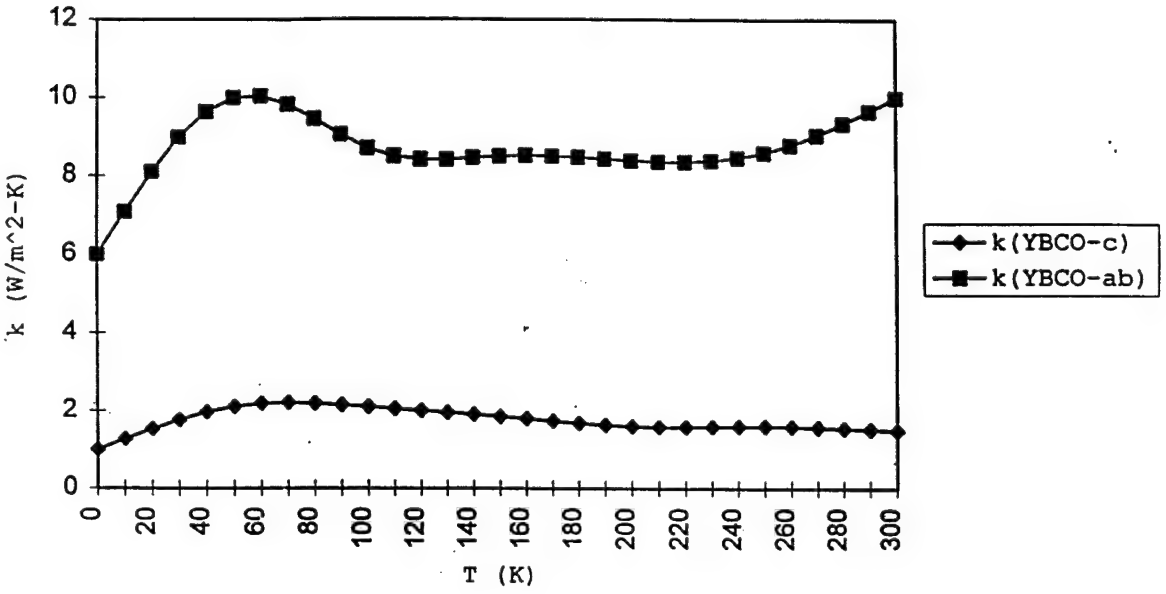

Figure 8. YBCO Thermal Conductivity

Values for temperature vs thermal conductivity for MgO are plotted in Figure 9 [Ref. 19]. Thermal conductivity for the MgO substrate is important not only for the error analysis, but also in the finite difference programs. Previous studies failed to use accurate values for thermal conductivity for both YBCO and MgO in their error analysis. This study utilizes cubic spline interpolation to the maximum extent possible to yield the best values for the thermal conductivities.

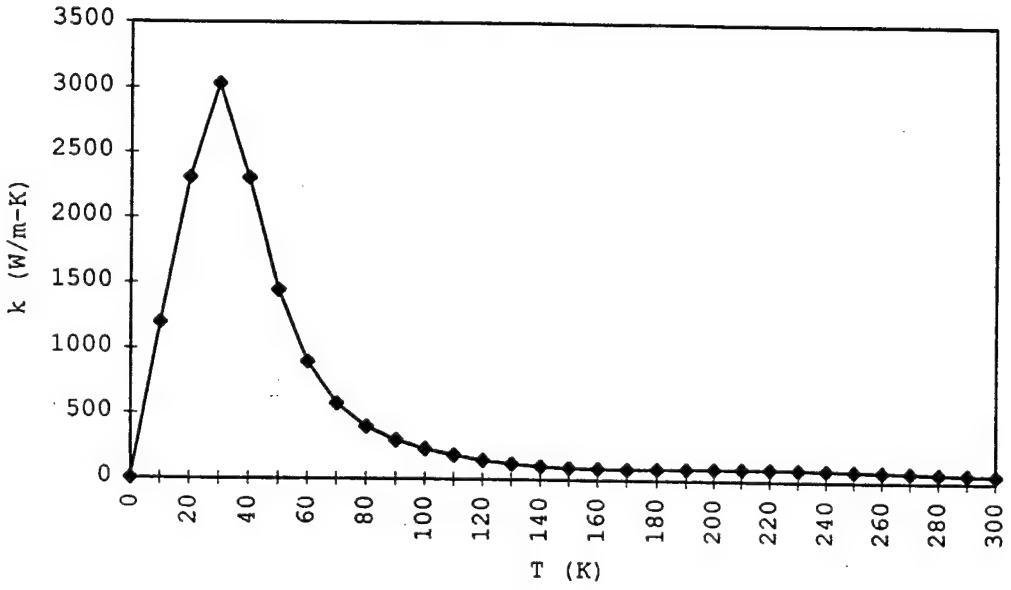

Figure 9. MgO Thermal Conductivity

III. EXPERIMENTAL

A. MATERIALS

The sample used for this study was an epitaxial $YBa_2Cu_3O_7$ thin film on a single-crystal MgO substrate. There are three steps in the fabrication process: film deposition, microfabrication by photolithography, and gold pad deposition for lead connection.

The films used in this study were purchased from Excell Superconductor. The $YBa_2Cu_3O_7$ film was deposited on the substrate by rf-magnetron sputtering. This sputtering process is fully described in Adachi et al. [Ref. 20] The MgO substrate thickness was 1 mm and the area was 10 mm x 10 mm. The $YBa_2Cu_3O_7$ film was 3000 Å (300 nm) thick. The film exhibited a critical temperature of $T_c \approx 78$ K during testing.

Etching was done by photolithography using a pattern drafted in AutoCAD 10 by polylines (Figure 10). The central region in Figure 10 was a result of the close spacing between the heater and sensor strips which caused them to appear to merge into one dark band. The AutoCAD pattern is converted into a mask by a pattern generator. The mask is a glass plate with the coated circuit, which resists the passage of ultraviolet light. Photoresist is spun onto the films and the mask steps the required circuit pattern optically onto the film [Ref. 21]. A standard developer is

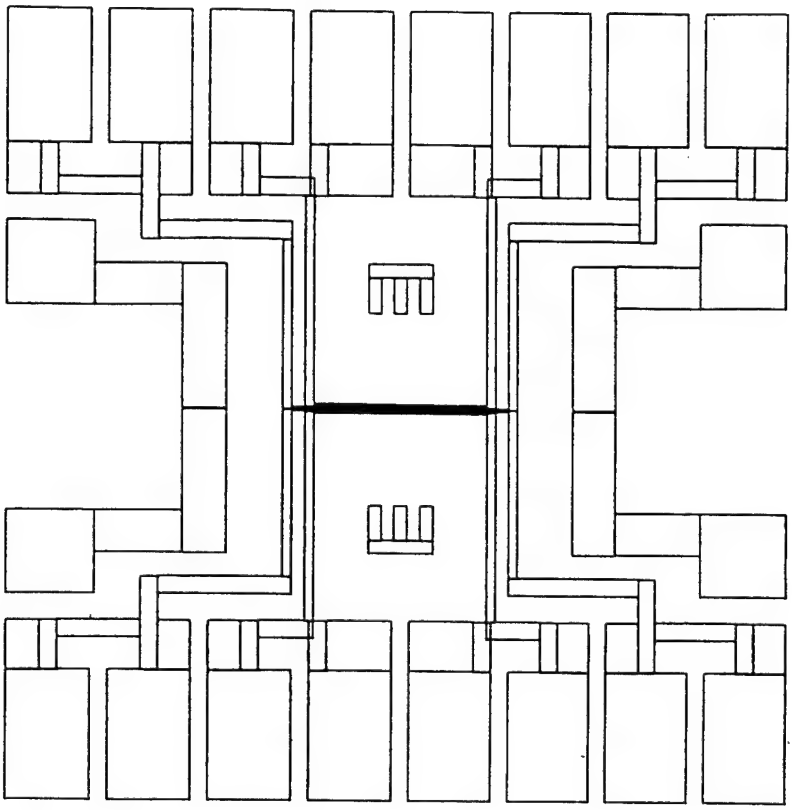

Figure 10. AutoCAD Pattern

then used to develop the photoresist to reveal the areas of the film to be etched. The etching solution is 1% H_3PO_4 (hypophosphoric acid) and the film is soaked for 15 minutes without agitation. The gap between the heater and the sensor strips is 0.01 mm which made etching difficult, however, high quality etching was accomplished. Detailed methods for etching YBCO films are given by Shin and Qiu [Ref. 22].

The connection pads to the etched film were deposited through a mask. The mask was fabricated out of polished and buffed sheet metal brass with holes to match the etched pattern. It was closely pressed onto the etched film, adjusted to match the pattern and taped in place. Gold, 1000 Å thick, was then deposited to form the connection pads. The resulting etched pattern with connection pads is shown in Figure 11. A 16-pin connector was then fabricated to allow electrical connection of the pads to the data acquisition unit while the sample was in the cryo-cooling apparatus.

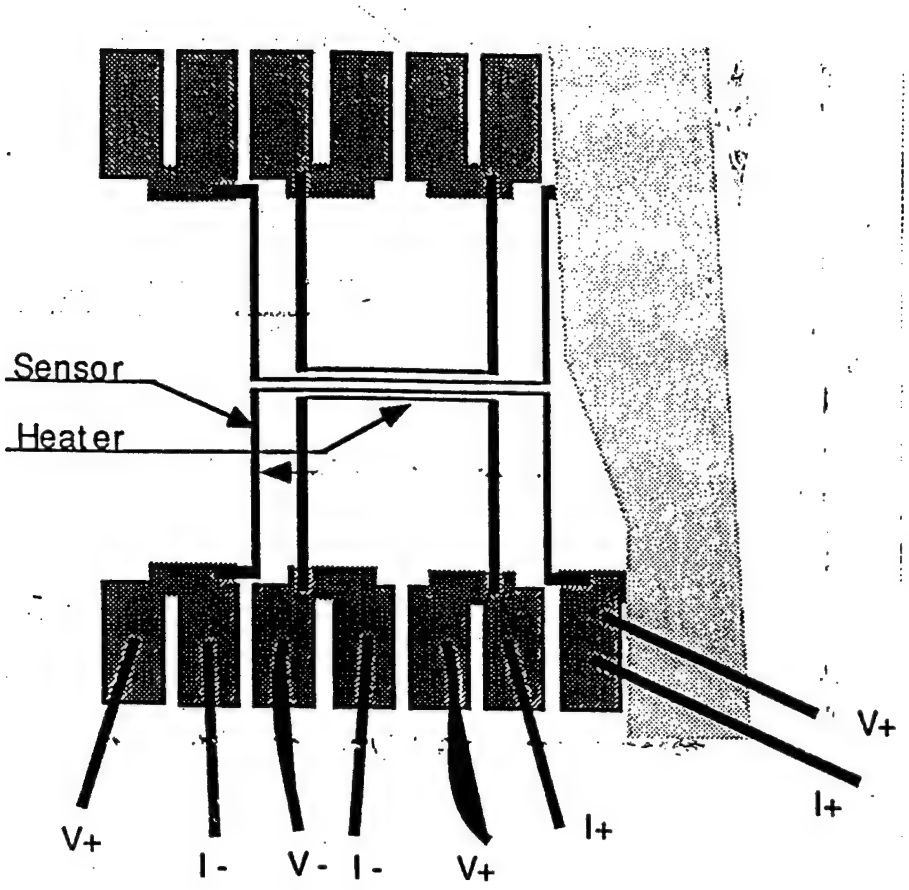

Figure 11. Etched Pattern with Connection Pads

B. EQUIPMENT

To prevent contaminants and moisture from condensing on the sample, experiments are conducted at a very high vacuum (10^{-6} torr). Operating at a high vacuum also reduces the thermal mass which the cryo-cooling equipment needs to cool and, most importantly, drastically reduces the heat leakage from the sample by convection in the chamber. The sample holder containing the sample is placed within a stainless steel hood (vacuum chamber) which is evacuated. Additionally, a brass shroud is provided between the sample holder and the stainless steel hood to reduce radiation loss during the process. The seal between the hood and the apparatus is accomplished with an O-ring and Dow Corning high vacuum grease. Figure 12 shows the experimental setup.

A CTI Cryogenics model 8001 (350 CP) cryo-cooler is used which can produce temperatures down to 19 K under good vacuum conditions (low cooling load). A diffusion pump is used in conjunction with the cryo-cooler and can achieve vacuums of up to 10^{-6} torr in about 2-3 hours. The pump is connected to a roughing pump for initial evacuation. The pump is cooled by water and supplemented by hand-poured liquid nitrogen. The vacuum level is measured by a hot-wire cathode gauge. The diffusion pump set up is shown in Figure 13.

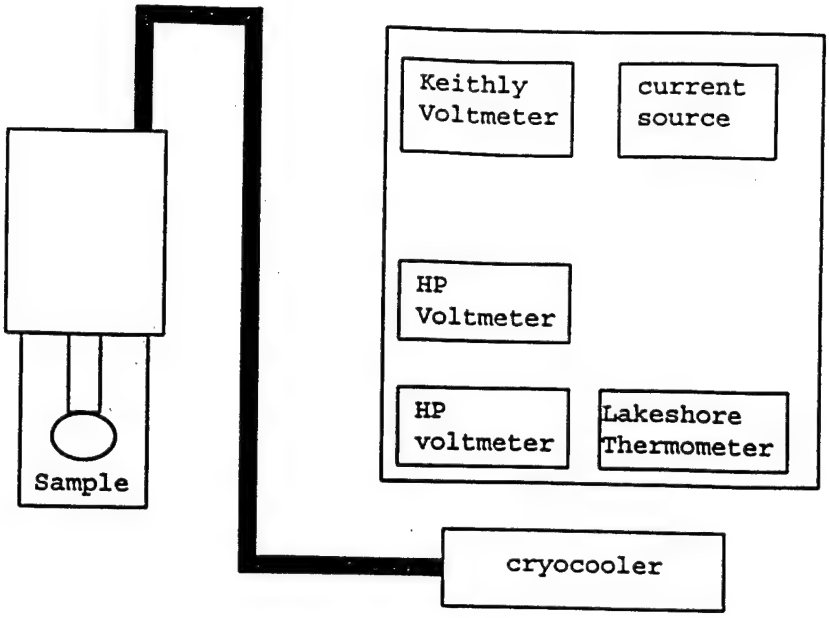

Figure 12. Experimental Setup

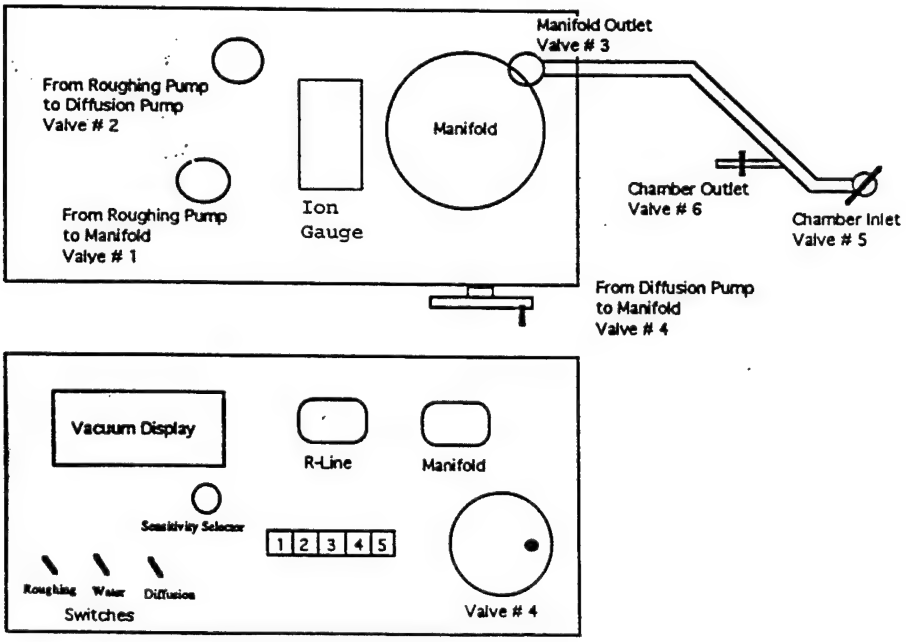

Figure 13. Diffusion Pump [Ref. 23]

A Keithley current source was used for the heater strip and the voltages are measured by a Keithley Nanovoltmeter. Previous experimental setups utilized a two-phase lock-in amplifier from EG&G to supply a small ac current for the sensor strip at a frequency of 47 HZ and lock onto the signal to measure voltage drop across the strip. This was found to introduce noise into the system and, consequently, the lock-in amplifier was removed from the circuit. All dc voltages across shunt resistors were measured with Hewlett Packard voltmeters.

In previous studies, data acquisition was accomplished using a Hewlett Packard computer with an HP basic program, however,this did not provide the operator with the ability to monitor important experimental parameters during the data taking. Monitoring and data acquisition for this study was accomplished on a Power Machintosh 8100/100 computer linked through an IEEE-488 interface. A Labview program was used to provide the operator with a visual display of heater resistance (ohms), sensor resistance (ohms) and coldfinger temperature (K). Additionally, digital readouts of heater current (ma), sensor current (ma), heater strip voltage (V) and sensor strip voltage (V) were displayed. The Labview program enabled better control of critical experimental parameters, such as coldfinger temperature, than were previously achievable and allowed the operator to view such events as the onset of superconductivity in the sample at T_c.

The thin film deposited on its substrate is mounted in a copper plug. The copper plug acts as a cold finger to conduct heat out from the bottom of the substrate. The design of the copper cold finger is shown in Figure 14. Apeizon-N thermal grease is used between the substrate and the copper block to ensure good thermal contact. The pin connector device is then screwed in place to make electrical connections from the sample to the data acquisition equipment. The copper cold finger plug is then screwed into the metallic chamber which is connected to the cryo-cooler.

C. PROCEDURE

The following procedure for measuring the thermal boundary resistance (R_b) between the film and the substrate is as described in Phelan et al. [Ref. 25]. Referring to Figure 15, two adjacent YBCO thin-film strips are used: one is used as the heater and one is used as the sensor. Four electrical contacts, including the voltage taps V^+_i and V^-_i, are made to each strip. This allows for independent four-point measurement of the resistance of each strip for various bias currents.

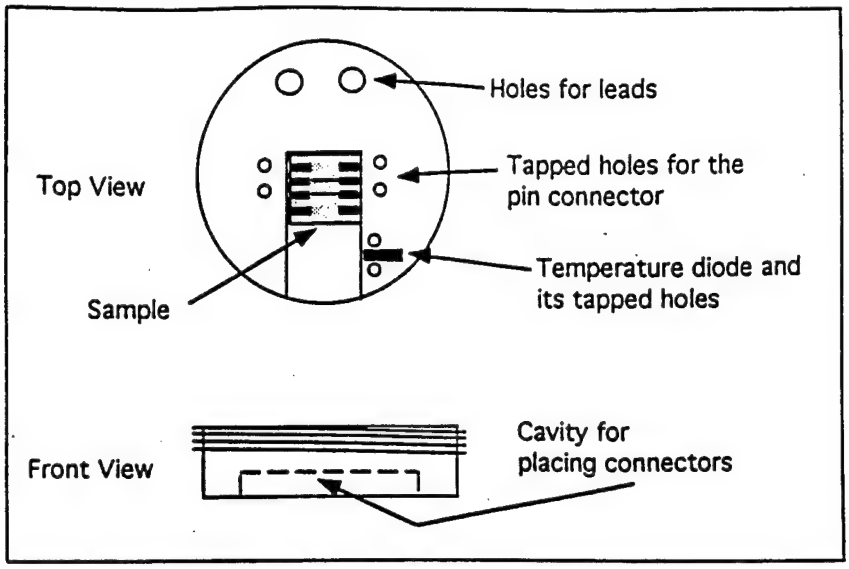

Figure 14. Copper Cold Finger [Ref. 24]

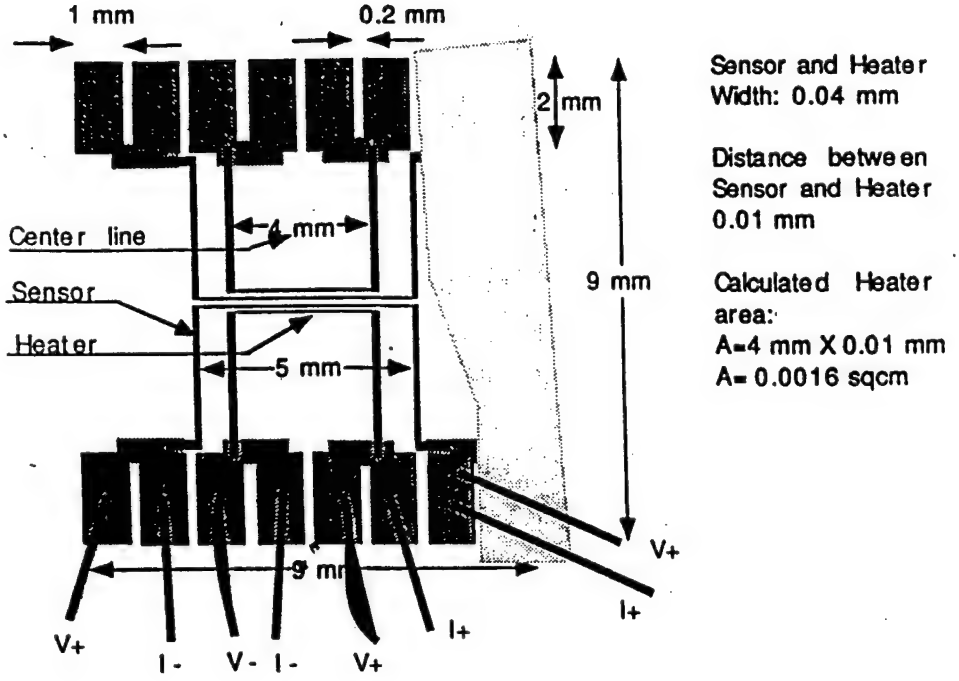

Figure 15. Electrical Connections

To measure the thermal boundary resistance between the heater strip and the substrate, a relatively large dc current is passed through the heater strip, while a much smaller sensing current ($I \leq 5\ \mu A$) is passed through the sensor strip. The Joule heating in the heater strip increases its temperature and the adjacent substrate temperature, and thus causes the temperature of the sensor strip to increase. Under steady-state conditions, R_b can be easily determined from the definition of the thermal boundary resistance

$$R_b = \frac{T_h - T_s}{q''} \qquad (1)$$

where T_h is the temperature of the heater strip and T_s the temperature of the substrate directly below the sensor strip. Heat flux, q'', is accurately calculated from the known heater voltage and current along with its contact area ($0.0016\ cm^2$) to give values in terms of W/cm^2. The temperature of the substrate below the heater strip is nearly equal to the temperature of the sensor strip, since the two strips are only separated by 0.01 mm.

Both T_h and T_s are determined from the steady-state values of their electrical resistances, which are considered to attain steady state when the subsequent data points change by less than 0.1%, after which the subsequent 10 points are averaged. After all data acquisition runs are completed, the sample is cooled to well below T_c, and the cryo-cooler is turned off. Temperature calibration curves for electrical resistance of the heater and sensor strips are determined by acquiring data as the sample slowly heats up to room temperature. Cubic spline interpolation is used to extract values of T_h and T_s from the temperature and resistance values acquired from the calibration curve. Calibration curves for one set of data are shown in Figure 16.

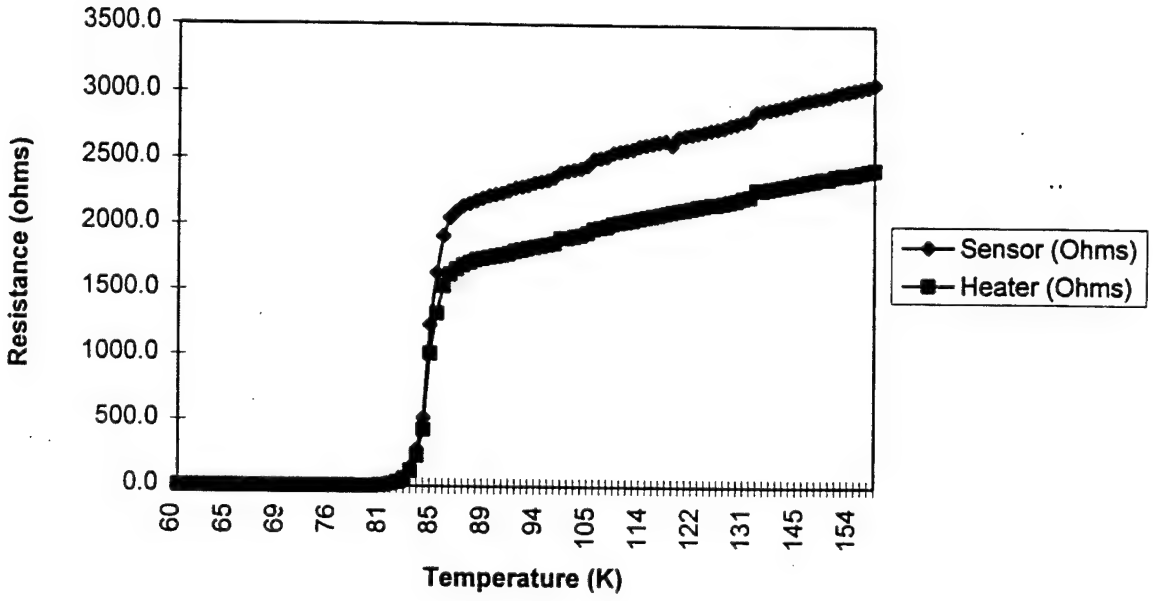

Figure 16. Calibration Curves

IV. RESULTS AND DISCUSSION

A. R_b CORRECTION

Values of R_b are calculated and tabulated for each data run. These values are calculated based on the assumption that the temperature of the substrate below the heater strip is nearly equal to the temperature of the sensor strip. The temperature difference for each data run must be corrected using the solution to the Laplace equation [Ref. 26].

The representative heat conduction problem is shown in Figure 17 and the solution to the Laplace equation is fully outlined in the Appendix I. The temperature distribution in the substrate is given by

$$T(x,y) = \sum_{n=1}^{\infty} C_n \cos\beta_n x \sinh\beta_n y \tag{2}$$

where

$$C_n = \frac{2q\sin\beta_n x_1}{k\beta_n^2 a \cosh\beta_n y} \tag{3}$$

and

$$T(x,b) = \sum_{n=1}^{\infty} \frac{2q\sin\beta_n x_1}{k\beta_n^2 a} \cos\beta_n x \tag{4}$$

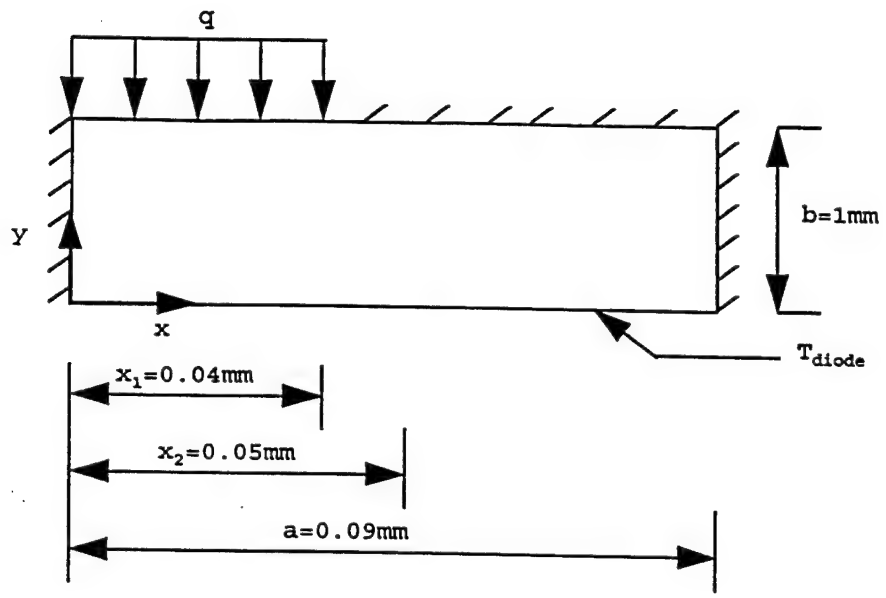

Figure 17. Representative Heat Conduction Problem

The temperature difference in the substrate between the heater and the sensor strip is given by

$$\Delta T=\sum_{n=1}^{\infty} \frac{2q\sin\beta_n x_1}{k\beta_n^2 a}\left(\frac{\sin\beta_n x_1}{x_1}+\frac{\sin\beta_n x_2}{a-x_2}\right) \tag{5}$$

which for the dimensions of the sample becomes

$$\Delta T=0.015\frac{q}{k} \tag{6}$$

The temperature in the substrate directly beneath the heater strip is found by adding the ΔT calculated from equation (6) to the measured sensor strip temperature (T_s):

$$T_{substrate}=T_s+\Delta T \tag{7}$$

Finally, the corrected value of R_b is found using

$$R_b=\frac{T_h-T_{substrate}}{q''} \tag{8}$$

Alternately, Swartz presents another method for determining $T_{substrate}$ [Ref. 27]. The temperature difference in the substrate can be found by integrating the Laplace equation using Laplace transforms.

The result is

$$\Delta T=\frac{qd}{\pi k}\left[\frac{(s-d)^2}{2d^2}\ln(s-d)+\frac{(s+d)^2}{2d^2}\ln(s+d)-\ln(d)-\frac{s^2}{d^2}\ln(s)\right] \quad (9)$$

where d is the width of the heater and sensor strips, and s is the separation between the strips from center to center. The resulting ΔT yields corrected R_b results that are consistent with those based on the ΔT calculated from equation (6).

Applying the ΔT obtained from equation (6), the corrected R_b is calculated. Figure 18 is a plot of T_s vs experimental and uncorrected values of R_b. As expected, the corrections are small and yield values of R_b that are slightly less than the experimental values. Uncertainty analysis must now be done on R_b for each data run.

B. UNCERTAINTY ANALYSIS

1. Uncertainty Equation

Consider Y which is a function of various parameters represented as follows

$$Y=f(x_1,x_2,\ldots,x_n) \quad (10)$$

where x_1, $x_2,\ldots,x_n$ are independent variables.

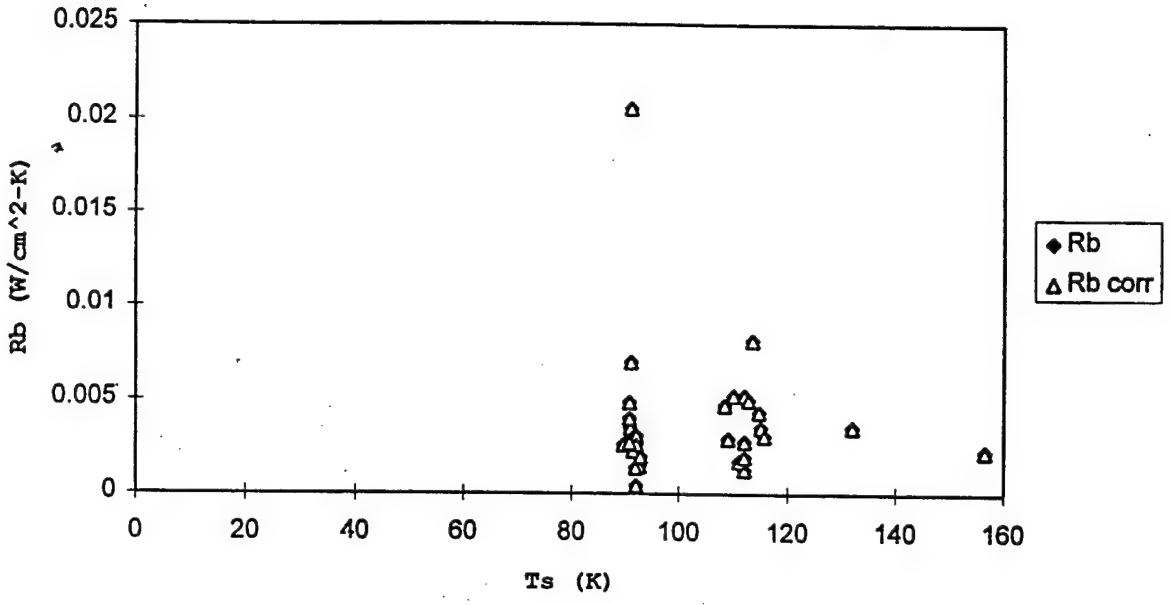

Figure 18. Experimental and Corrected Values of R_b

The uncertainty, u_f, in Y can be written as [Ref. 28]

$$u_Y=[(u_{x_1}\frac{\partial f}{\partial x_1})^2+u_{x_2}(\frac{\partial f}{\partial x_2})^2+\ldots+u_{x_n}(\frac{\partial f}{\partial x_n})^2]^{0.5} \quad (11)$$

where u_{x1}, u_{x2}, ..., u_{xn} are the uncertainties in measuring x_1, x_2, ..., x_n, respectively.

The uncertainty for R_b is given by

$$u_{R_b}=[(u_{\Delta T}\frac{\partial f}{\partial \Delta T})^2+u_{q''}(\frac{\partial f}{\partial q''})^2]^{0.5} \quad (12)$$

$$=[(u_{\Delta T}\frac{1}{q''})^2+(u_{q''}\frac{-\Delta T}{q''^2})^2]^{0.5}$$

2. Temperature Difference Uncertainty

The temperature difference is given by $\Delta T=T_h-T_s$, and its uncertainty is given by

$$u_{\Delta T}=[(u_{T_h})^2+(u_{T_s})^2]^{0.5} \quad (13)$$

The temperatures T_h and T_s are obtained from the calibration curves for the electrical resistances of the heater and the sensor strips. Previous studies divided the calibration curves up into sections and performed a polynomial fit on them to obtain equations for the curves. The uncertainty was then estimated from the standard deviation of the difference between the calibration data points and the fitted curves.

The present study uses cubic spline interpolation to determine the desired resistance value from the calibration data, thus eliminating the need for curve fitting. The uncertainties for T_h and T_s are therefore reduced to the uncertainty of the Si diode temperature sensor (± 0.1K). The resulting uncertainty for ΔT from equation (13) is ± 0.14K.

3. Heat Flux Uncertainty

Uncertainty in the heat flux results from uncertainty in the heat transferred from the heater strip into the substrate. The heat transferred into the substrate is the measured heat transfer minus conduction and radiation losses:

$$q_{heater} = q_{measured} - q_{cond\ losses} - q_{rad\ losses} \tag{14}$$

Its uncertainty is

$$u_{q_{heater}} = [(u_{q_{measured}})^2 + (u_{q_{cond\ losses}})^2 + (u_{q_{rad\ losses}})^2]^{0.5} \tag{15}$$

The uncertainty for $q_{measured}$ is equal to the uncertainty in the power applied to the heater strip ($q = E_{heater} I_{heater}$), which is

$$u_{q_{measured}} = [(u_E I)^2 + (u_I E)^2]^{0.5} \tag{16}$$

The uncertainties u_E and u_I are taken as the uncertainties for measuring voltage and current which are ± 1%.

The uncertainty for $q_{conduction\ loss}$ is expressed as the percentage of $q_{measured}$ which is conducted through the film lead to the substrate, and along the film lead and through the pin connector. Figure 19 shows the possible heat conduction paths and Figure 20 shows the thermal circuit with the resistances along the conduction paths.

Referring to Figure 20, the thermal resistance across the YBCO heater film is defined as $R_{film,htr}$ and the resistance across the substrate below the film as $R_{sub,htr}$. The resistance across the substrate below the film lead is designated $R_{sub,lead}$. The resistance along the film lead is defined as $R_{film\ lead}$.

The conductive thermal resistances are given by

$$R=\frac{\Delta T}{q}=\frac{\Delta T}{q''\cdot A}=\frac{\Delta z}{k\cdot A} \tag{17}$$

where

Δz is the thickness

k is the thermal conductivity

A is the heat transfer area

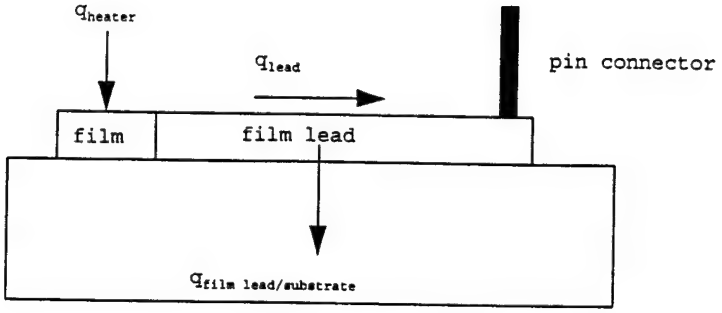

Figure 19. Heat Conduction Paths

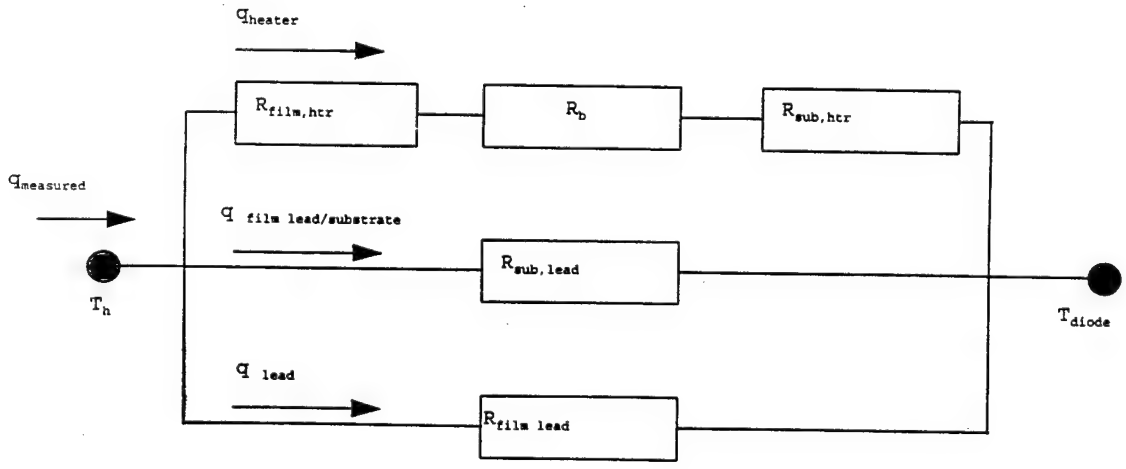

Figure 20. Thermal Circuit

The physical dimensions and thermal conductivities used to calculate the thermal resistances are given in Table 1. The ratio of the heat flows is determined from the ratio of the total resistances in the three branches of the thermal circuit. The values of thermal conductivities and branch resistances are from analysis of a typical data run at T_s = 91 K.

The value for $R_{film\ lead}$ is very high in comparison with the other resistance values and, consequently, the dominant heat leakage in the film lead is through the substrate. Thus, referring to Figure 21, we need to determine $x_{critical}$ at which the ratio $q_{film\ lead/substrate}$ and $q_{lead/pin\ connector}$ is sufficiently high (taken as 0.5).

For the film lead of length x and width w, resistance between the film lead and substrate and, the resistance along the film can be written as

$$R_{film\ lead/subtrate} = \frac{t}{k_{MgO} w x} \tag{18}$$

$$R_{film\ lead} = \frac{x}{k_{YBCO_{ab}} w d} \tag{19}$$

Parameter	Values		Resistances	Magnitudes
k_{YBCO} c-direction	2.1496 W/m-K		$R_{film,htr}$	87.431 K/W
k_{YBCO} ab-plane	9.0496 W/m-K		R_b x area under film	5.608×10^{-6} K/W
k_{MgO}	295.66 W/m-K		$R_{sub,htr}$	2212 K/W
Film Thickness	300×10^{-9} m		$R_{sub,\ lead}$	9915 K/W
Length of Heater Film	0.04×10^{-3} m			
Area of Substrate Under Heater	0.0016×10^{-4} m^2		$R_{film\ lead}$	19830 K/W
Length of Film Lead (avg)	7×10^{-3} m		R_{pin}	0.002 K/W
Width of Film Lead (avg)	$.08 \times 10^{-3}$ m			
Total Area of Film Lead	0.56×10^{-6} m^2			
Thickness of Substrate	10^{-3} m			

Table 1. Error Analysis Values

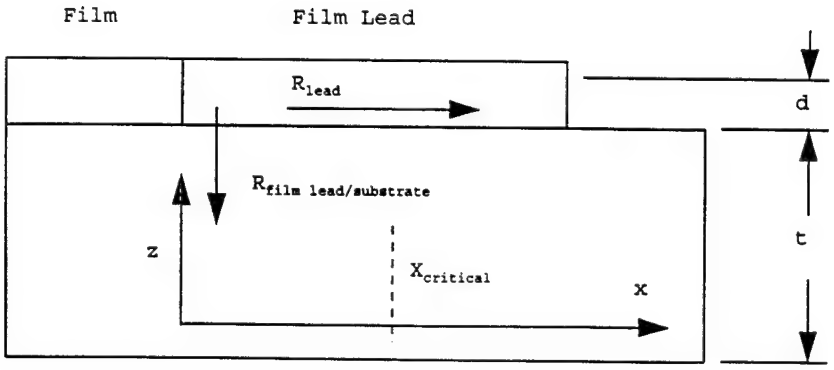

Figure 21. Film Lead Heat Leakage Paths

This yields a ratio of $q_{film\ lead/substrate}$ to $q_{lead/pin\ connector}$ of

$$\frac{q_{film\ lead/substrate}}{q_{film\ lead}} = \frac{x^2 k_{MgO}}{k_{YBCO_{ab}} dt} \tag{20}$$

Upon assigning a value of 0.50 to the ratio, the value for $x_{critical}$ becomes 2.143 mm, which gives us a value for $R_{sub,lead}$ of 19830 K/W and $R_{film\ lead}$ of 9915 K/W. R_1, R_2 and R_3 are defined as the total branch resistances for q_{heater}, $q_{film\ lead/substrate}$ and q_{lead} respectively.

The ratio of the heat leakage to the heat supplied to the heater is

$$\beta = \frac{q_{film\ lead/substrate} + q_{lead/pin\ connector}}{q_{heater}} = \frac{R_1}{\left(\frac{1}{R_2} + \frac{1}{R_3}\right)^{-1}} = 0.29 \tag{21}$$

which gives a percentage heat loss due to conduction of

$$\frac{q_{film\ lead/substrate} + q_{lead/pin\ connector}}{q_{film\ lead/substate} + q_{lead/pin\ connector} + q_{heater}} \cdot 100 = \frac{0.29}{1.29} \cdot 100 = 22.7\% \tag{22}$$

It is reemphasized that the values for R_b and the thermal conductivities used in this calculation were from a typical data run. Individual data points will be evaluated using their specific information to obtain their uncertainty values.

4. Radiation Loss Uncertainty

Part of the heat from the film radiates to its surroundings, which is the cold head holder. The cold head holder is assumed to be at T_{diode} and the resistance due to radiation heat transfer is determined. This evaluation is done using the Stefan-Boltzmann law to calculate the heat flux between T_{heater} and T_{diode}.

$$q''=\varepsilon\sigma\,[T^4_{heater}-T^4_{diode}] \tag{23}$$

where

$q''\equiv$ heat flux from the film to the cold head holder

$\epsilon \equiv$ emissivity of the film taken as 1

$\sigma \equiv$ Stefan-Boltzmann constant (5.6697×10^{-8} W/m^2-K^4)

Expanding the term $[T^4_{heater}-T^4_{diode}]$ in equation (23),

$$q''=\varepsilon\sigma\,[T^2_{htr}-T^2_{diode}]\,[T^2_{htr}+T^2_{diode}] \tag{24}$$

$$q''=\varepsilon\sigma\,[T_{htr}+T_{diode}]\,[T_{htr}-T_{diode}]\,[T^2_{htr}+T^2_{diode}] \tag{25}$$

$$q''=\varepsilon\sigma\,[T_{htr}+T_{diode}]\,[T^2_{htr}+T^2_{diode}]\,\Delta T \tag{26}$$

Using typical experimental values for T_{heater} and T_{diode} and the film area associated with the heater strip, a resistance value for radiative heat transfer is calculated between the heater strip and the cold head holder using

$$R_{radiative}=\frac{T_{heater}-T_{diode}}{q''\cdot A} \tag{27}$$

and the resulting value of $R_{radiative}$ is given by

$$R_{radiative}=\frac{1}{\epsilon\sigma\,(T_{htr}+T_{diode})\,(T^2_{htr}+T^2_{diode})\,A} \tag{28}$$

The value for $R_{radiative}$ is found to be on the order of 10^4 K/W. The values for $R_{radiative}$ are at least one order of magnitude greater than the values for $R_{sub,htr}$. Consequently, radiation losses are not included in the thermal resistance network or error analysis considerations.

5. Uncertainty in R_b

The values of R_b are plotted in Figure 22 against T_s showing error bars for each data point. As anticipated the error in each value is minimal. Having used cubic spline interpolation for the values of T_h and T_s, errors due to temperature measurements in previous studies have been eliminated.

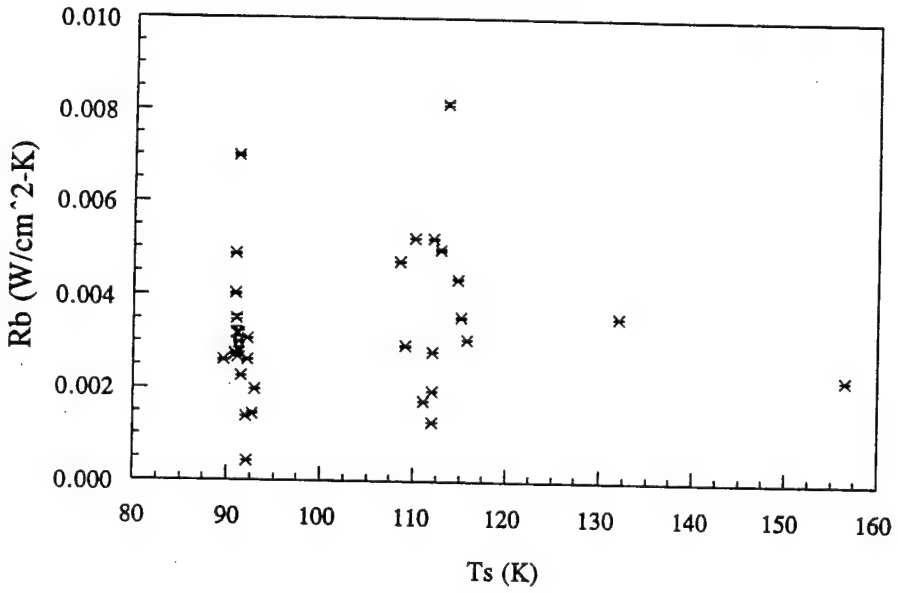

Figure 22. R_b Error

C. R_b VARIATION WITH HEAT FLUX

Having completed the error analysis, a plot of T_s vs the corrected values of R_b is shown in Figure 23 without error bars. Referring to the plot, the values for R_b with varying heat flux are shown for the data taken at average values of T_s equal to 91.2, 91.5, 110.8 and 113.6 K. Values acquired at 134 and 157.5 K are also shown.

It is clear from the plot that the majority of R_b values over the entire range of T_s are between 0.005 and 0.001 W/cm^2-K. Despite varying the values of heat flux at the different values of T_s, no discernable dependency of R_b on heat flux can be observed from this plot. Examining R_b from an different perspective, heat flux vs R_b is plotted in Figure 24.

The plot of heat flux vs R_b also shows no overall trend in R_b as heat flux is varied. Given that the variations in heat flux in this study were done to explore hysteresis effects, it is apparent that the individual hysteresis runs themselves must be plotted to observe any trends of R_b with heat flux. The individual hysteresis runs may reveal that just as important as the current value of heat flux is, heat flux history of the sample may be equally important.

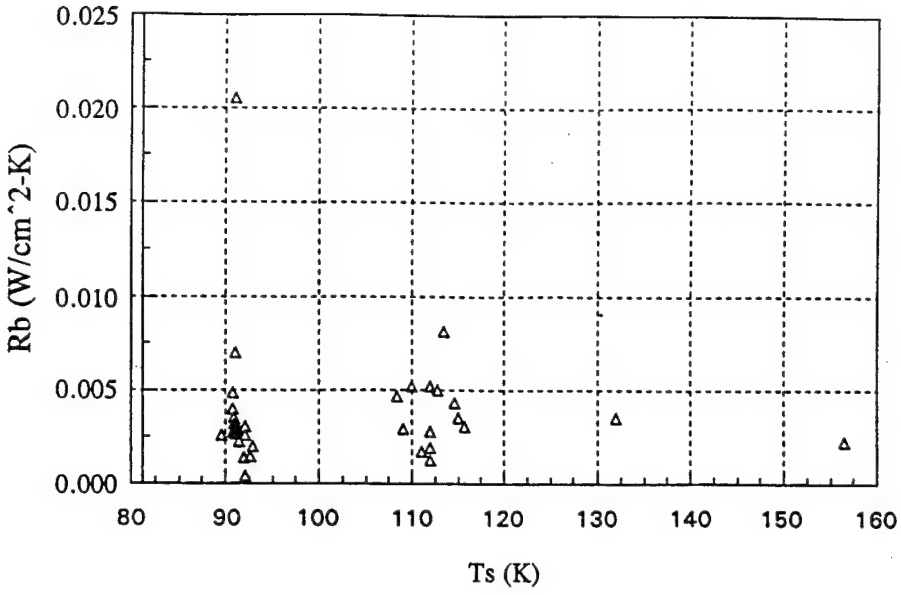

Figure 23. T_s vs $R_{b\ corrected}$

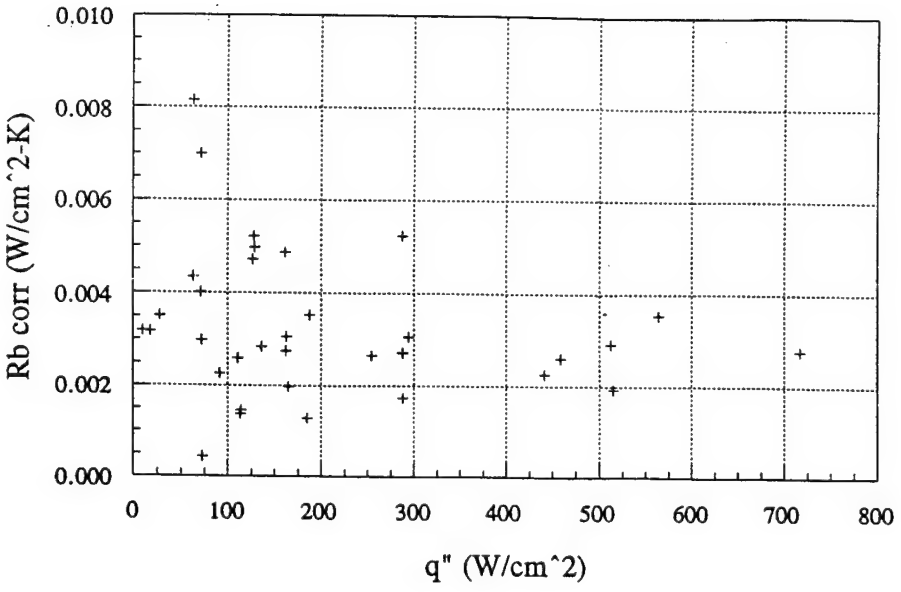

Figure 24. Heat Flux vs Rb corrected

D. HYSTERESIS EFFECTS

Cycling of the heat flux at fixed values of T_s was performed to determine if there were any hysteresis effects on R_b. Values of T_s = 91.2, 91.5, 110.8, 113.6K were used during these data runs. Plots of Heat Flux vs R_b were generated and are shown in Figures 25 through 28. Arrowheads are used on the plots to show the direction in which heat flux was varied.

Based on the plots alone, the conclusion may be drawn that R_b does display some sort of hysteresis effect when heat flux is varied to a maximum and back to a minimum. However, for similar values of T_s (i.e., 91.2 and 91.5 K / 110.8 and 113.6K), the hysteresis pattern displayed is not consistent. This is especially noted at the T_s values of 91.2 and 91.5 K where the values used for heat flux were very well matched. However, with all the hysteresis runs, the starting value of R_b is always greater than the finishing values of R_b. This effect is believed to be stress related and two hypotheses are proposed.

First, it has been shown that the film peeling stress, that is, the normal stress at the film/substrate interface, becomes more negative (i.e., more compressive) with increasing q" [Ref. 30]. This increase in compressive stress causes a decrease in R_b, as seen in Figures 22 through 25. As q" is reduced from its maximum value, some of that high

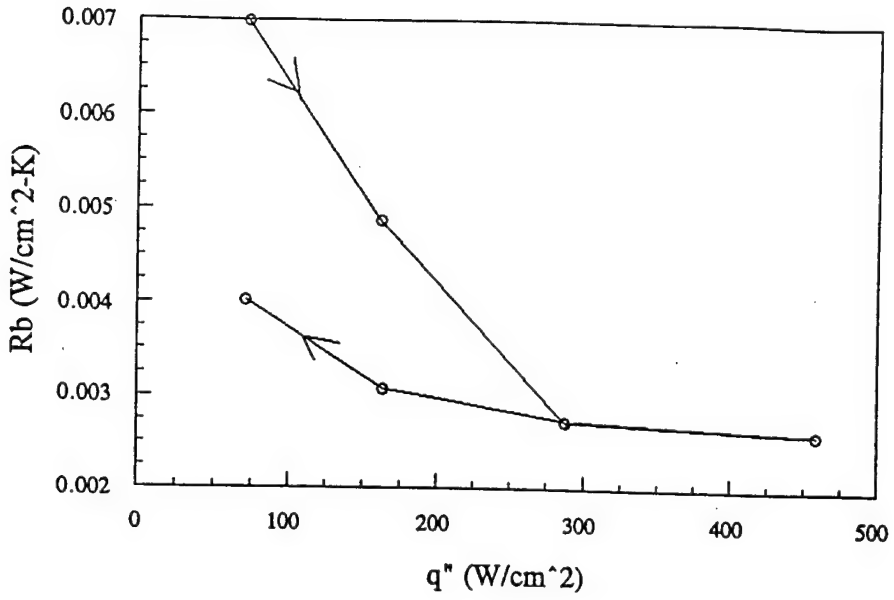

Figure 25. Hysteresis Effects at $T_{s\ average}$ = 91.2 K

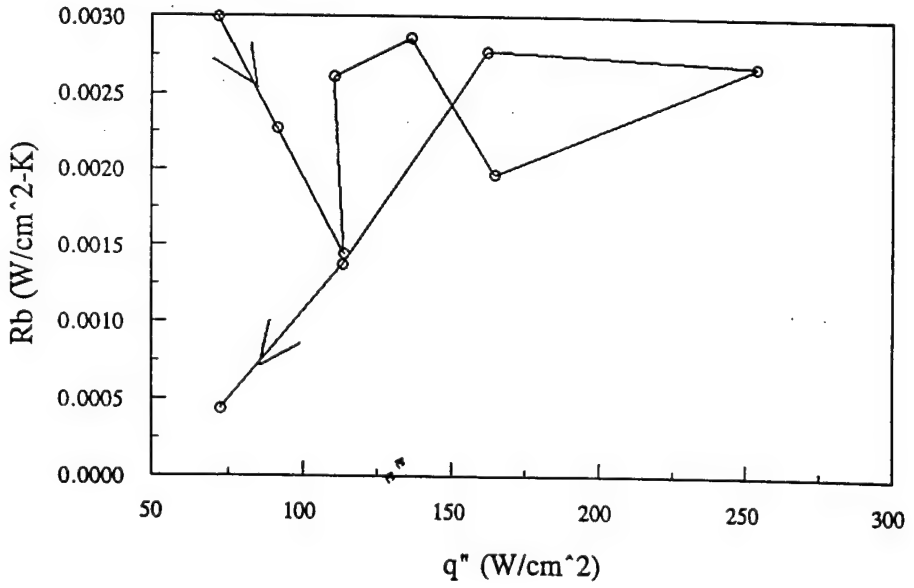

Figure 26. Hysteresis Effects at $T_{s\ average}$ = 91.5 K

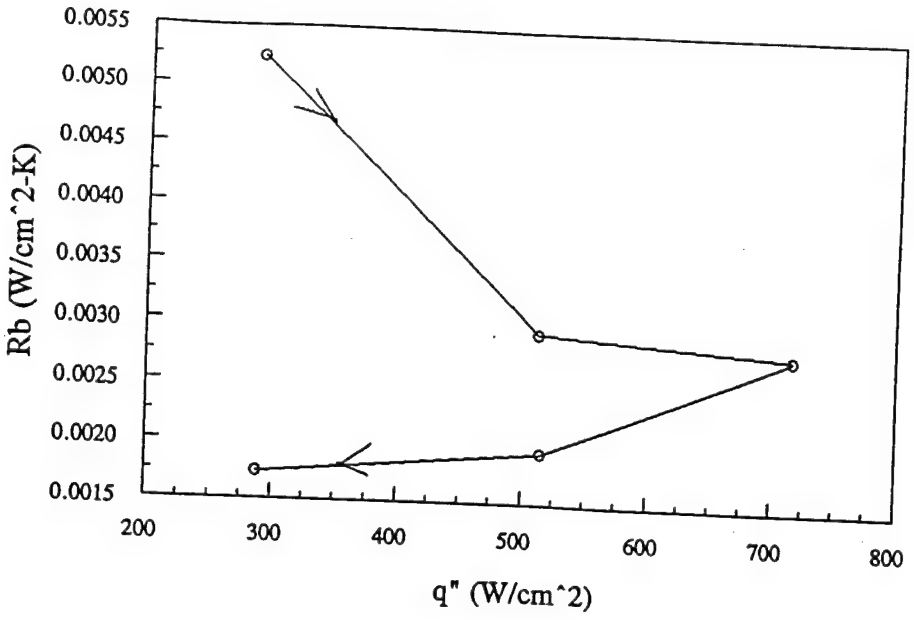

Figure 27. Hysteresis Effects at $T_{s\ average}$ = 110.8 K

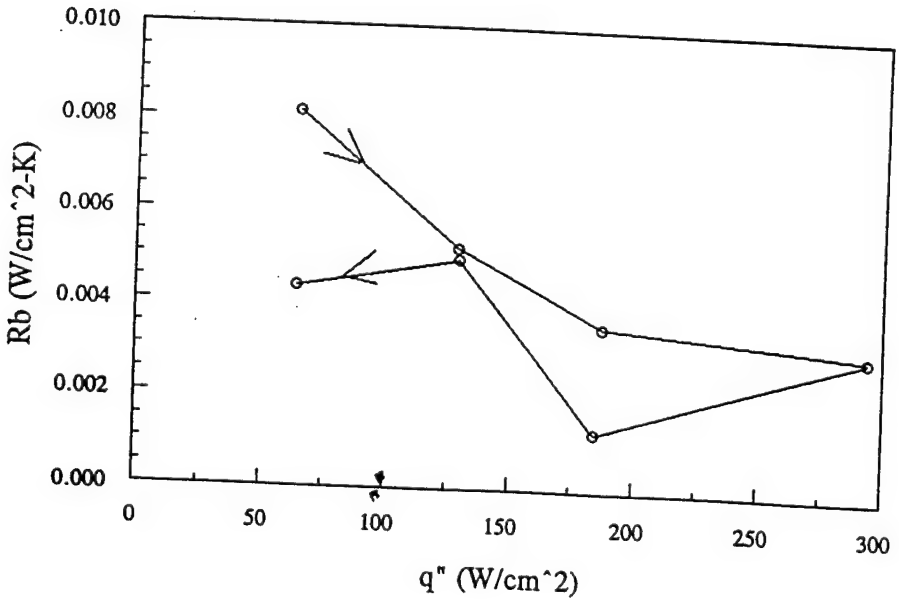

Figure 28. Hysteresis Effects at $T_{s\ average}$ = 113.6 K

compressive stress may not be relieved, leaving the film with a greater compressive (negative) peeling stress than the original condition, and thus a lower final R_b compared to the initial R_b. Second, as a result of the increasing compressive stress, microstructural changes are produced near the film/substrate interface. These are microstructural changes, such as the movement of vacancies or other defects, which do not change back as the stress is relieved. These changes in the microstructure will affect the microscale heat transfer characteristics between the film and the substrate reflecting in the changes in R_b observed.

It is known that YBCO displays a hysteresis effect on its thermal conductivity upon heating and cooling [Ref. 30]. However, the presence of this effect cannot be determined from the hysteresis runs. What is clear is that control of variables in the process is crucial to determining the presence of hysteresis effects.

Current experimental techniques used in this study control T_s by manually cycling the cryo cooler on and off in an attempt to maintain the temperature T_s. Although the Lab View program will not acquire data until steady state is reached, duplication of conditions from one data run to the next is not possible. Considering the hysteresis run at an average value of T_s = 91.2 K, the standard deviation of T_s is 0.92 K. This results in a variation in thermal

conductivity of YBCO in the c-plane from 2.146 to 2.138 W/m-K and a variation in the thermal conductivity of MgO from 277.27 to 290.86 W/m-K. This effect resulting from poor control of T_s is, in itself, enough to mask any true hysteresis effects that may be present. This serves to emphasize the importance of controlling the experimental parameters.

As a direct result of this study, the cryo cooling apparatus currently being designed will use an electric heater to control the temperature. In conjunction with the Lab View program, the resistance value of the sensor will be controlled. A constant sensor resistance displayed by Lab View represents a constant value of T_s. The Lab View program additionally allows the control of heater current and voltage to obtain the desired power input. Thus, having attained positive control over the substrate temperature and the heat flux, duplication of experimental conditions will be possible. Subsequent data runs, no matter what the purpose, should yield more useable data.

E. FINITE DIFFERENCE METHODS

In an effort to predict values of R_b under different experimental conditions, finite difference numerical techniques were used to model the physical situation. The control volume method illustrated in Figure 29 was used in conjunction with a graded network to model the film and substrate [Ref. 31, 32]. Using these techniques, two different programs were written using Microsoft Fortran Version 5.1 to arrive at a solution using the Gauss-Siedel method: one based solely on temperature distribution and one using both temperature constraints and heat input [Ref 33].

Focusing only on the temperature distribution within the substrate, a graded network was designed as illustrated in Figure 30; the program listing is contained in Appendix B. Program inputs are T_h, T_s and T_{diode} which yield outputs of R_b experimental, R_b calculated and temperature distribution within the substrate. The grading of the network was controlled by programming the spacing of the nodes in both the I and J directions. Tolerance between previous node values and calculated values is also inputted. The program initializes all nodes to T_{diode} and then imposes T_h and T_s on the network and subsequently iterates until convergence within the prescribed tolerance between the current and the previously calculated values.

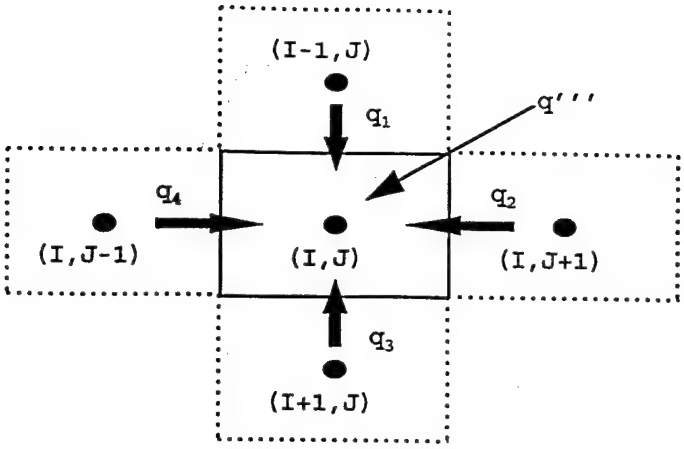

Figure 29. Finite Difference Control Volume

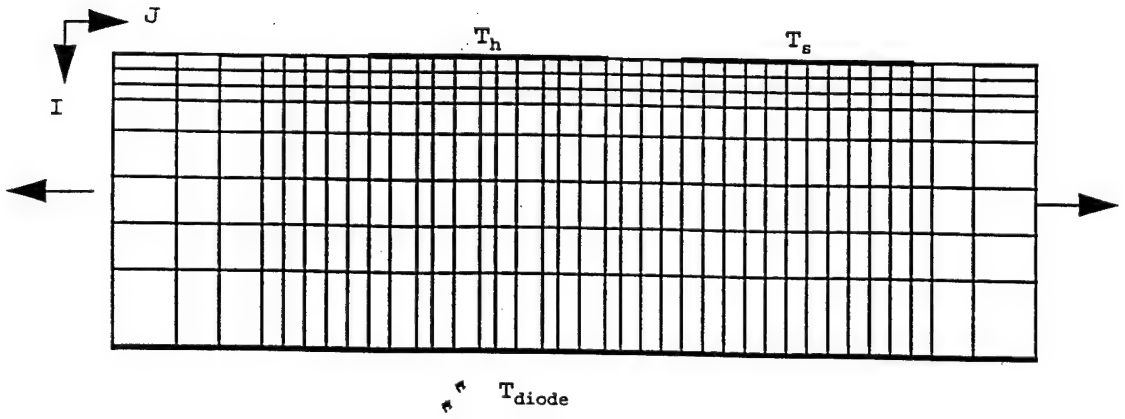

Figure 30. Temperature Distribution Graded Network

Figures 31 and 32 show the contour plots generated for inputted temperature values of T_h=92.8 K, T_s=92.6 K and T_{diode}=85.5 K resulting from iteration based on temperature. The contour plots provide a qualitative insight into the temperature distribution in the substrate. Temperature contours emanate from the heater strip and rapidly drop off to values approaching T_{diode}. Consequently, with substrate dimensions of 10 mm^2 by 1 mm thick, the heat affected zone is very small. Figure 31 displays a substrate thickness of 0.2 mm from the heater strip and Figure 32 displays a substrate thickness of 0.04 mm from the heater strip.

In addition to the temperature distribution, upon inputting experimental values for T_h, T_s and T_{diode}, the temperature difference between the heater strip and the substrate directly beneath was calculated. Temperatures for the nodes in the substrate directly beneath the heater strip are averaged. The temperature difference between the heater strip and the substrate was calculated using T_h and this average value. It is this temperature difference that the program uses with the heat flux to calculate the values of R_b. These values are typically within 1 order of magnitude of the actual experimental values, but do not accurately predict the experimental values.

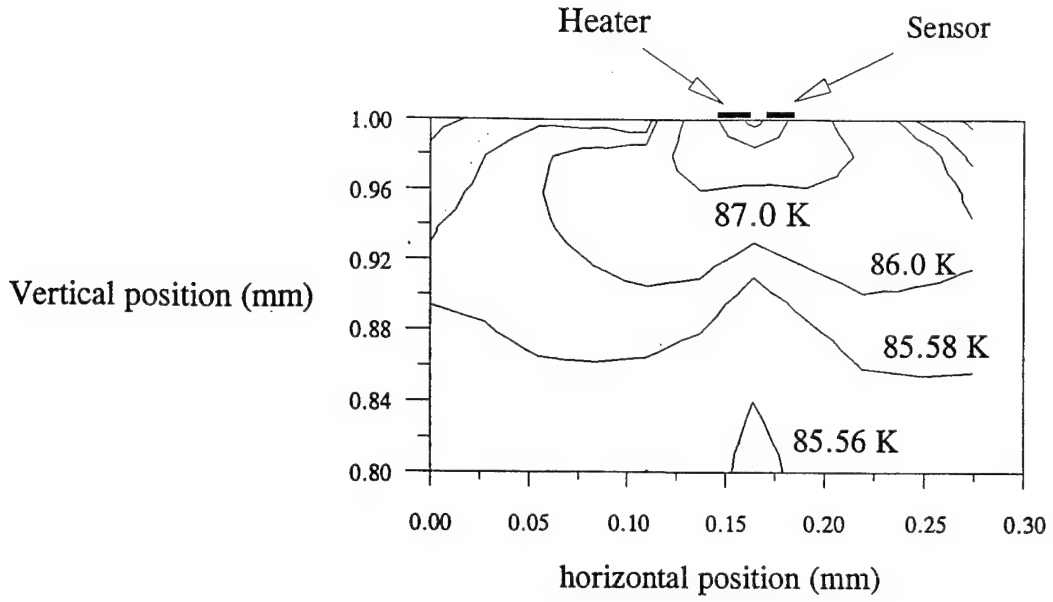

Figure 31. Substrate Heat Affected Zone

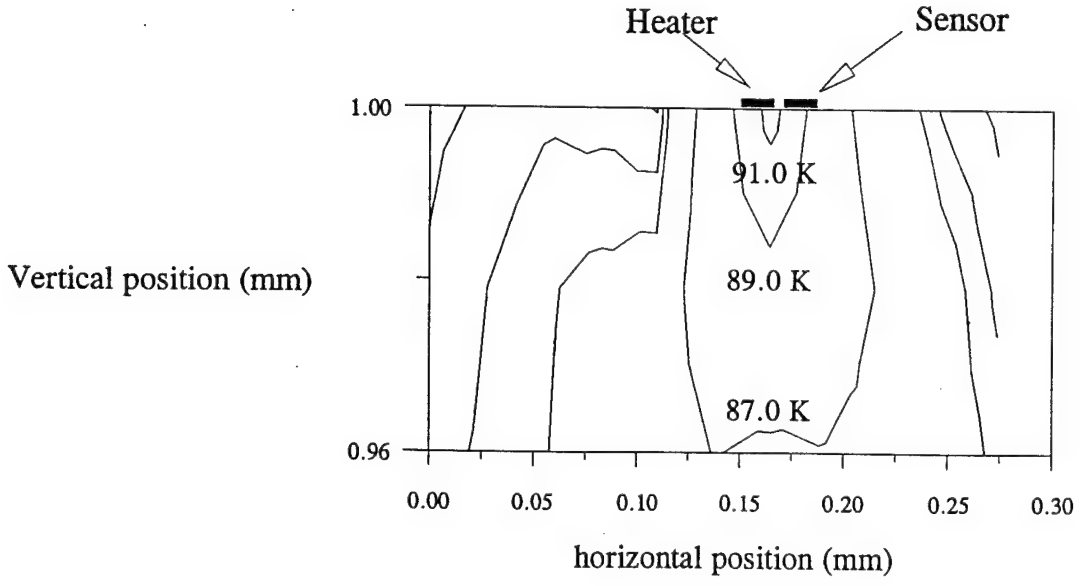

Figure 32. Temperature Distribution Close to the Heater

To provide a mechanism for inputting heater power into the program, the temperature distribution program was modified. The program proceeded as before iterating on temperature until convergence was achieved. Then the constraint of holding the heater temperature at T_h is removed and heat generation is introduced to apply the appropriate power to the heater strip. The resulting adjustment in node temperatures yielded values of R_b calculated on the order of 10^{-5} W/cm^2-K, which is far less than any of the experimental values of R_b generated.

It is believed that the large discontinuity in thermal conductivities at the interface of the heater and the substrate results in temperatures being driven to lower values. In addition, Microsoft Fortran running on a PC has a limitation of approximately 60 by 60 nodes of memory. This was a severe limitation because the program results were found to be very sensitive to grid size. The memory limitation precluded performing an in depth grid sized sensitivity study. In an attempt to overcome the averaging effect on the thermal conductivity that results from the finite difference method of solution and the limitations on grid size, a new program was written. Given that the heated affected zone is small compared to the size of the substrate and that the sensor strip produces no joule heating, symmetry was used. A centerline was passed through the heater strip and only half the substrate was modeled as

illustrated in Figure 33. The program functioned in the same manner as the previous program, however, the heater strip was modeled by numerous layers of nodes instead of just one layer of nodes in an attempt to overcome the averaging effects. Despite these efforts, the new program still yielded values for R_b on an order of magnitude of 10^{-5} W/cm^2-K. Once again, the results were very sensitive to grid size.

Poor results from the finite difference programs are certainly contributed to by the inability to use a small enough grid size. However, an inability to model factors such as microscale heat transfer effects, changes in peeling stress of the thin film and factors included in the acoustic mismatch theory probably also contributed to the disparity between experimental and calculated values. The purpose and the premise of the program are valid. Consequently, restructuring the program for more grid-sized flexibility using a main frame computer is certainly warranted.

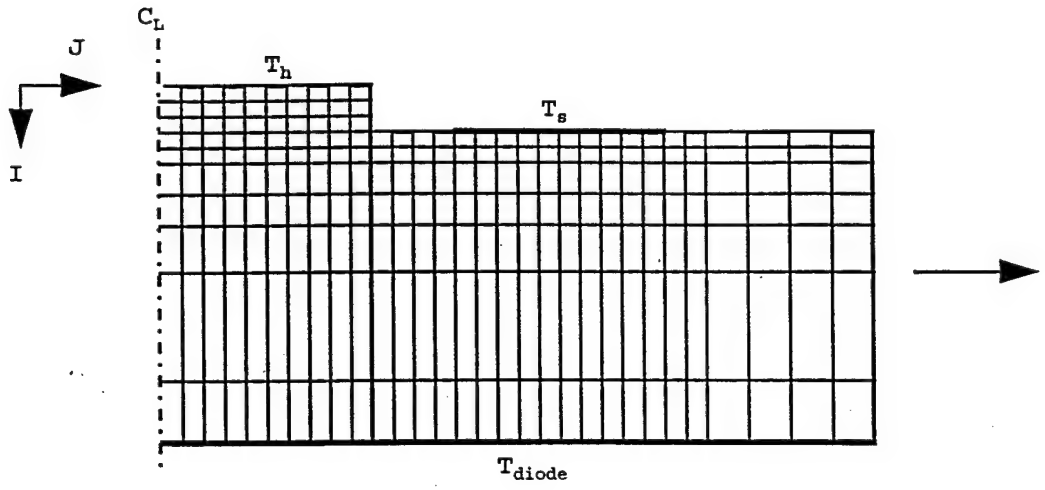

Figure 33. Symmetric Model of the Substrate

V. RECOMMENDATIONS

This study has focused on process improvement. The use of the new straight line etching pattern, elimination of the lock-in amplifier, use of a pin connector and the Lab View program have certainly improved the data acquisition process. Utilization of the cubic spline interpolation for determining heater and sensor strip temperatures has eliminated the largest source of error from previous studies which was the ΔT calculation. However, further improvement in parameter control is needed. Utilization of the heater in the cryo cooler to control the resistance of the sensor strip and, consequently, substrate temperature is essential.

Once substrate temperature control is achieved, data runs can be duplicated to a reasonable level of assurity. All data runs from this study should then be redone. Particularly the hysteresis runs where we have some indication of the hysteresis effects being present but, due to poor parameter control, the results are inconclusive. In addition, it is recommended that fatigue runs be done as well. Cycling heat flux between fixed values in a repetitive manner may indicated whether film failure or progressive changes in R_b will occur under intermittent service use.

It is recommended that the finite difference program be redone on a main frame. This would remove limitations due to computer memory. Additionally, finite element methods should

be employed if possible. Modeling the geometry and varying the grid size could be done with much greater flexibility using a finite element program. The ability to model the physical situation on the computer is important. Given the amount of time in the lab that it takes to acquire data, the program could be a valuable tool for planning data acquisition runs.

In closing, the control of experimental parameters and computer modeling should be used in the performance of further heat flux variation studies. Re-running past experiments must be done to establish a consistent record of R_b variation. In addition, further areas of heat flux variation, such as fatigue affects must be studied.

APPENDIX A. SUBSTRATE TEMPERATURE DISTRIBUTION

Referencing Figure 14 and using the heat conduction equation for two dimensional steady state heat transfer we get [Ref. 34],

$$\frac{\partial^2 T}{\partial x^2}+\frac{\partial^2 T}{\partial y^2}=0 \qquad (1)$$

with the boundary conditions (BC):

(i) $@\,x=0$ $\qquad \frac{\partial T}{\partial x}=0$

(ii) $@x=a$ $\qquad \frac{\partial T}{\partial x}=0$

(iii) $@x=a$ $\qquad T=0$

(iv) $@y=b$ $\qquad \frac{\partial T}{\partial y}=f(x)$

$$\text{where } f(x)=\begin{cases}\frac{q}{k} & 0<x<x_1\\ o & x_1<x<a\end{cases}$$

Boundary condition (iii) is defined for Figure 14 to make the problem homogeneous:

$$T=T'-T_{diode} \tag{2}$$

where T' is the actual temperature distribution. Since we are interested in the actual temperature distribution (ΔT), equation 2 can be ignored later.

The solution for equation (1) is given by

$$T=X\cdot Y$$

where

$$X=C_1\cos\beta x+C_2\sin\beta x \tag{3}$$

$$Y=C_3\cosh\beta y+C_4\sinh\beta y \tag{4}$$

such that

$$\frac{dX}{dx}=-C_1\beta\sin\beta x+C_2\beta\cos\beta x \tag{5}$$

$$\frac{dY}{dy}=-C_3\beta\sinh\beta y+C_4\cosh\beta y \tag{6}$$

BC (i) and (5) gives

$$C_2=0$$

BC (ii) and (5) gives

$$-C_1\beta\sin\beta a=0$$

$$\Rightarrow \beta_n=n\pi \Rightarrow \beta_n=\frac{n\pi}{a} \tag{7}$$

From BC (iii) and (4)

$$C_3=0$$

Hence

$$T=C_n\cos\beta_n x\sinh\beta_n y \tag{8}$$

and BC (iv) and (6) give

$$\frac{\partial T}{\partial y}=C_n\beta_n\cos\beta_n x\sinh\beta_n y=f(x) \tag{9}$$

Using the orthogonality property we get

$$\int_0^a f(x)\cos\beta_n x dx=\int_0^a C_n\beta_n\cosh\beta_n b\cos^2\beta_n x dx$$

$$LHS=\int_0^{x_1}\frac{q}{k}COS\beta_n x dx+\int_{x_1}^a 0\cdot\cos\beta_n x dx$$

$$LHS=[\frac{1}{\beta_n}\frac{q}{k}\sin\beta_n x|_o^{x_1}=\frac{q}{k\beta_n}\sin\beta_n x_1 \qquad (10)$$

and

$$RHS=C_n\beta_n y\int_0^a \cos^2\beta_n x dx$$

$$=C_n\beta_n\cosh\beta_n y\int_o^a \frac{\cos 2\beta_n x+1}{2}dx$$

$$=C_n\beta_n y[\frac{1}{2}\frac{\sin 2\beta_n x}{2\beta_n}+\frac{1}{2}]_0^a$$

$$=C_n\beta_n\cosh\beta_n y\cdot\frac{a}{2}$$

$$RHS=\frac{a}{2}C_n\beta_n\cosh\beta_n y \qquad (11)$$

Equating the LHS to the RHS

$$\frac{q}{k\beta_n}\sin\beta n x_1=\frac{a}{2}C_n\beta_n\cosh\beta_n y$$

Thus

$$C_n = \frac{2q\sin\beta_n x_1}{k\beta_n^2 a\cosh\beta_n y} \tag{12}$$

and

$$T = \sum_{n=1}^{\infty} C_n \cos\beta_n x \sinh\beta_n y$$

$$T = \frac{2q\sin\beta_n x_1}{k\beta_n^2 a\cosh\beta_n y} \cos\beta_n x \sinh\beta_n y \tag{13}$$

The temperature difference between the area below the heater strip and the sensor strip is given by the difference between the mean temperatures under each strip.

The mean temperature below the heater strip is

$$T_{1mean} = \frac{\int_0^{x_1} T dx}{\int_0^{x_1} dx} = \sum_{n=1}^{\infty} \left[\frac{2q\sin\beta_n x_1 \sin\beta_n x}{k\beta_n^2 a \beta_n x_1} \right]$$

$$T_{1mean} = \sum_{n=1}^{\infty} \frac{2q\sin\beta_n x_1 \sin\beta_n x_1}{k\beta_n^3 a x_1} \Big|_o^{x_1} \tag{14}$$

The mean temperature below the sensor strip is

$$T_{2mean}=\frac{\int_{x_2}^{a} T dx}{\int_{x_1}^{a} dx}=\sum_{n=1}^{\infty}\frac{1}{(a-x_2)}\left[\frac{2q\sin\beta_n x_1 \sin\beta_n x}{k\beta_n^2 a\beta_n}\right]_{x_2}^{a}$$

$$T_{1mean}=-\sum_{n=1}^{\infty}\frac{2q\sin\beta_n x_1 \sin\beta_n x_2}{k\beta_n^3 a(a-x_2)} \qquad (15)$$

The temperature drop is then calculated as

$$\Delta T=T_{1mean}-T_{2mean}$$

$$\Delta T=\sum_{n=1}^{\infty}\frac{2q\sin\beta_n x_1 \sin\beta_n x_1}{k\beta_n^3 a x_1}+\sum_{n=1}^{\infty}\frac{2q\sin\beta_n x_1 \sin\beta_n x_2}{k\beta_n^3 a(a-x_2)}$$

$$\Delta T=\sum_{n=1}^{\infty}\frac{2q\sin B_n x_1}{k\beta_n^3 a}\left(\frac{\sin\beta_n x_1}{x_1}+\frac{\sin\beta_n x_2}{a-x_2}\right) \qquad (16)$$

The series converges and is approximated for n=3. From equation (7) and the values of the constants from Figure 14 equation (16) becomes

$$\delta T = 0.0154 \frac{q}{k} \tag{17}$$

Using the experimental values from each data run in conjunction with the value of T_s a corrected value of R_b is calculated.

APPENDIX B. FINITE DIFFERENCE PROGRAM

```
C     TEMPERATURE DISTRIBUTION OF A THIN FILM ON A SUBSTRATE
C     SOLUTION BY GAUSS-SEIDEL ITERATION METHOD

C      INTEGER I,J,LI,LJ
      INTEGER L
      PARAMETER(LI=57,LJ=59)
      DIMENSION PX(LI,LJ), PY(LI,LJ), T(LI,LJ) ,TTEMP(LI,LJ)
      REAL DISTX, DX, DISTY, D2, D3, XA, YA, DIFF, TOLL,
      KS,KF
      OPEN(UNIT=10, FILE='CONTOUR', STATUS='UNKNOWN')
C     DEFINE TOLERANCE
      TOLL=0.005

      P= .182383
      Th=92.837
      Ts=92.672
      Tcf=85.55
      X=(Th+Ts)/2
      KF=2.605-0.00506*X

      KS=2283.61772-39.9669583*X+0.245369913*X**2
      -0.00050878108*X**3

C     DEFINE X AND Y NODE POSITIONS

C     DEFINE 1ST ROW X POSITIONS
      DISTX=0.0
      DO 10 J=1,LJ
C     DEFINE TOP ROW SPACING USING IF STATEMENTS
      IF(J.LE.15) DX=0.01
      IF((J.GE.16).AND.(J.LE.49)) DX=0.001
      IF(J.GT.49) DX=0.01


C     WRITE PX AND PY FOR J POSITION
      PX(1,J)=DISTX
      PY(1,J)=0.0

C     ESTABLISH SPACING FOR THE J+1 POINT
      DISTX=DISTX+DX
10    CONTINUE

C     EXPAND 1ST ROW POSITIONS INTO Y POSITIONS

      DO 20 I=2,LI
      DO 30 J=1,LJ
         PX(I,J)=PX(1,J)
         IF(I.EQ.2) DISTY=0.00001
         IF(I.EQ.3) DISTY=0.00001
```

```
            IF(I.EQ.4) DISTY=0.00001
            IF(I.EQ.5) DISTY=0.00001
            IF(I.GT.5) DISTY=0.01
            IF(I.GT.51)DISTY=0.1
            PY(I,J)=PY(I-1,J)+DISTY
30       CONTINUE
20       CONTINUE

C        INITIALIZE T(I,J) THE TEMPERATURE ARRAY
         DO 50 I=1,LI
         DO 60 J=1,LJ
            T(I,J)=Tcf
60       CONTINUE
50       CONTINUE

         DO 52 J=16,31
        T(1,J)=Th
52       CONTINUE
         DO 53 J=36,49
        T(1,J)=Ts
53       CONTINUE

C        USE GAUSS-SEIDEL ITERATIVE TECHNIQUE TO CALCULATE THE
C        TEMPERATURES

C        SET THE ITERATION COUNTER N=1 FOR THE FIRST ITERATION;
         SET THE
C        TOLERANCE COUNTER K=0
         N=1
         L=0
         PRINT*,'L=',L
55       K=0

C        CALCULATE VALUES FOR THE HEATER STRIP
         IF (L.EQ.0) GOTO 59

         DO 57 J=16,31
         D3=PY(2,J)-PY(1,J)
         XA=(PX(1,J+1)-PX(1,J-1))/2
c        compensate power for the size of the control volume
         q=P*1000*(0.1/.16)

C         KS=2893.84258-657.933*(92.754-30)**0.337
C       KS=100*7762.715*92.754**(-1.6941479)
         KTOT=(KS+KF)/(KS*KF)
         TTEMP(1,J)=T(2,J)+(q*D3*KTOT)/(XA*2)

         DIFF=ABS(TTEMP(1,J)-T(1,J))
         IF((DIFF-TOLL).GT.0.) K=K+1
         T(1,J)=TTEMP(1,J)
```

```
57     CONTINUE

C      UPPER LEFT HAND CORNER NODE
59     PRINT*,'GO TO 59'
       D2=PX(2,2)-PX(2,1)
       D3=PY(3,1)-PY(2,1)
       XA=D2/2.
       YA=D3/2.

       TTEMP(2,1)=(YA*D3*T(2,2)+XA*D2*T(3,1))/(YA*D3+XA*D2)
       DIFF=ABS(TTEMP(2,1)-T(2,1))

       IF((DIFF-TOLL).GT.0.) K=K+1

       T(2,1)=TTEMP(2,1)

C      TOP EDGE NODE

       DO 70 J=2,LJ-1

       IF((J.GE.16).AND.(J.LE.31)) GOTO 75
       IF((J.GE.36).AND.(J.LE.49).AND.(L.EQ.0)) THEN
       GOTO 75
       END IF
       D2=PX(2,J+1)-PX(2,J)
       D3=PY(3,J)-PY(2,J)
       D4=PX(2,J)-PX(2,J-1)

       XA=(D2+D4)/2.
       YA=D3/2.


      TTEMP(2,J)=(YA*D3*D4*T(2,J+1)+XA*D2*D4*T(3,J)
      +YA*D2*D3*T(2,J-1))
      +/(YA*D3*D4+XA*D2*D4+YA*D2*D3)

       GOTO 65

75     I=2
       D1=PY(I,J)-PY(I-1,J)
       D2=PX(I,J+1)-PX(I,J)
       D3=PY(I+1,J)-PY(I,J)
       D4=PX(I,J)-PX(I,J-1)

       XA=(D2+D4)/2
       YA=(D1+D3)/2

C       KF=5.0
C       KS=2893.84258-657.933*(92.754-30)**0.337
```

```
      TTEMP(I,J)=(2*XA*KF*D2*D3*D4*T(I-1,J)
     ++YA*D1*(KS+KF)*D3*D4*T(I,J+1)
     ++XA*D1*(KS+KF)*D2*D4*T(I+1,J)
     ++YA*D1*(KS+KF)*D2*D3*T(I,J-1))/
     +(2*XA*KF*D2*D3*D4+YA*D1*(KS+KF)*D3*D4
     ++XA*D1*(KS+KF)*D2*D4+YA*D1*(KS+KF)*D2*D3)

65    DIFF=ABS(TTEMP(2,J)-T(2,J))
      IF((DIFF-TOLL).GT.0.) K=K+1

      T(2,J)=TTEMP(2,J)

70    CONTINUE

C     UPPER RIGHT HAND CORNER NODE

      D3=PY(3,LJ)-PY(2,LJ)
      D4=PX(2,J)-PX(2,J-1)

      XA=D4/2.
      YA=D3/2.


TTEMP(2,LJ)=(XA*D4*T(3,LJ)+YA*D3*T(2,LJ-1))/(XA*D4+YA*D3)
      DIFF=ABS(TTEMP(2,LJ)-T(2,LJ))
      IF((DIFF-TOLL).GT.0.) K=K+1

      T(2,LJ)=TTEMP(2,LJ)

C     SET UP DO LOOP TO CALCULATE LH, INTERIOR AND RH NODES
      FROM
C     I=3 (ROW 3) UNTIL I=LI-1 (NEXT TO LAST ROW)

      DO 80 I=3,LI-1

C     LEFT HAND SIDE NODES

      D1=PY(I,1)-PY(I-1,1)
      D2=PX(I,2)-PX(I,1)
      D3=PY(I+1,1)-PY(I,1)

      XA=D2/2.
      YA=(D1+D3)/2.


      TTEMP(I,1)=(XA*D2*D3*T(I-1,1)+YA*D1*D3*T(I,2)
     +XA*D1*D2*T(I+1,1))/
     +(XA*D2*D3+YA*D1*D3+XA*D1*D2)
      DIFF=ABS(TTEMP(I,1)-T(I,1))
      IF((DIFF-TOLL).GT.0.) K=K+1
```

```
      T(I,1)=TTEMP(I,1)

C     INTERIOR NODES

      DO 90 J=2,LJ-1

      D1=PY(I,J)-PY(I-1,J)
      D2=PX(I,J+1)-PX(I,J)
      D3=PY(I+1,J)-PY(I,J)
      D4=PX(I,J)-PX(I,J-1)

      XA=(D2+D4)/2.
      YA=(D1+D3)/2.

      TTEMP(I,J)=(XA*D2*D3*D4*T(I-1,J)+YA*D1*D3*D4*T(I,J+1)
     ++XA*D1*D2*D4*T(I+1,J)+YA*D1*D2*D3*T(I,J-1))/
     +(XA*D2*D3*D4+YA*D1*D3*D4+XA*D1*D2*D4+YA*D1*D2*D3)

      DIFF=ABS(TTEMP(I,J)-T(I,J))
      IF((DIFF-TOLL).GT.0.) K=K+1

      T(I,J)=TTEMP(I,J)

90    CONTINUE

C     RIGHT HAND SIDE NODES

      D1=PY(I,LJ)-PY(I-1,LJ)
      D3=PY(I+1,LJ)-PY(I,LJ)
      D4=PX(I,LJ)-PX(I,LJ-1)

      XA=D4/2.
      YA=(D1+D3)/2.

      TTEMP(I,LJ)=(XA*D3*D4*T(I-1,LJ)+XA*D1*D4*T(I+1,LJ)
     ++YA*D1*D3*T(I,LJ-1))/(XA*D3*D4+XA*D1*D4+YA*D1*D3)
      DIFF=ABS(TTEMP(I,LJ)-T(I,LJ))
      IF((DIFF-TOLL).GT.0.) K=K+1

      T(I,LJ)=TTEMP(I,LJ)

80    CONTINUE

      IF ((K.EQ.0).AND.(L.EQ.1)) THEN
      PRINT*,'T(2,25)=',T(2,25),'     K=',K
      GO TO 100

      END IF
      IF(K.EQ.0) THEN
      L=1
      N=1
```

```
      PRINT*,'GOTO 55'
C     GO TO 55
      GO TO 100

      ELSE
      PRINT*,'T(2,25)=',T(2,25),'     K=',K

      N=N+1
      GO TO 55
      END IF


100   DO 105 I=1,26
      DO 110 J=1,LJ
      WRITE(10,102)I,J,PX(I,J),1-PY(I,J),T(I,J)
102   FORMAT(1X,I4,I4,3F12.8)
110   CONTINUE
105   CONTINUE
      PRINT*,'L=',L
      PRINT*,'N=',N

      Th=0
      DO 107 J=16,31
     TAVG=Th+T(1,J)
     Th=TAVG
107   CONTINUE
      Th=TAVG/16
      PRINT*,'Th=',Th

      Tc=0
      DO 108 J=16,31
     TAVG=Tc+T(2,J)
     Tc=TAVG
108   CONTINUE
      Tc=TAVG/16
      PRINT*,'Tc=',Tc

      Rb=(Th-Tc)/(P/0.0016)
      DELT=Th-Tc
      PRINT*,'DELTA T=',DELT
      PRINT*,'Rb=',Rb
      Rbexp=(Th-Ts)/(P/0.0016)
      PRINT*,'Rbexp=',Rbexp
      PRINT*,'KS=',KS
      END
```

LIST OF REFERENCES

1. Ruggiero, S.T. and Rudman, D.A., 1990, Superconducting Devices, Academic Press, Inc., San Diego, CA., pp. xi-xii.

2. Phelan, P.E., Song, Y., Nakabeppu, O., Ito, K., Ohmori, T., and Torikoshi, K., 1994, "Film/Substrate Thermal Boundary Resistance For An Er-Ba-Cu-O High-T_c Superconducting Film", Journal of Heat Transfer, Vol. 116, No. 4, pp. 1038-1041.

3. Phelan, P.E., Song, Y. and Kelkar, M., 1994, "Film/Substrate Thermal Boundary Resistance of Er-Ba-Cu-O High T_c Thin Films", Ceramic Transactions, Vol. 41, Symposium on Grain Boundaries and Interfaces in Electronic Ceramics, 1993 PAC RIM Meeting of the American Ceramic Society. Levinson, L.M. and Hirano, S. eds. pp. 307-314.

4. Little, W.A., 1959,"The Transport of Heat Between Dissimilar Solids At Low Temperatures", Canadian Journal of Physics, Vol. 37, p. 334.

5. Swartz, E.T. and Pohl, R.O., 1989,"Thermal Boundary Resistance", Reviews of Modern Physics, Vol. 61, No. 3, July, pp. 618-620.

6. Kelkar, M., 1995, "Thermal Boundary Resistance in High Temperature Thin-Film Superconductors", Master's Thesis, University of Hawaii, p. 19.

7. Burkhard, G., Sawaoka, A.B. and Phelan, P.E., 1995, "The Effect of Umklapp-Processes on the Heat Transport of Solids: Evaluation of the Thermal Boundary Resistance of Two Joined Solids", Presented at The Symposium on Thermal Science and Engineering in Honor of Chancellor Chang-Lin Tien, San Francisco, CA, November 14, 1995, p. 2.

8. Burkhard, G., Sawaoka, A.B. and Phelan, P.E., 1995, "The Effect of Umklapp-Processes on the Heat Transport of Solids: Evaluation of the Thermal Boundary Resistance of Two Joined Solids", Presented at The Symposium on Thermal Science and Engineering in Honor of Chancellor Chang-Lin Tien, San Francisco, CA, November 14, 1995, p. 8.

9. Phelan, P.E., Song, Y., Nakabeppu, O., Ito, K., Ohmori, T., and Torikoshi, K., 1994, "Film/Substrate Thermal Boundary Resistance For An Er-Ba-Cu-O High-T_c Superconduction Film", Journal of Heat Transfer, Vol. 116, No. 4, pp. 1038-1041.

10. Swartz, E.T. and Pohl, R.O., 1989,"Thermal Boundary Resistance", Reviews of Modern Physics, Vol. 61, No. 3, July, pp. 616-617.

11. Phelan, P.E., Song, Y., Nakabeppu, O., Ito, K., Ohmori, T., and Torikoshi, K., 1994, "Film/Substrate Thermal Boundary Resistance For An Er-Ba-Cu-O High-T_c Superconduction Film", Journal of Heat Transfer, Vol. 116, No. 4, pp. 1038-1041.

12. Incropera, F.P. and DeWitt, D.P., 1985, Fundamentals of Heat and Mass Transfer, 2nd ed., John Wiley & Sons, New York, NY, pp. 142-156.

13. James, M.L., Smith, G.M., Wolford, J.C., 1985, Applied Numerical Methods for Digital Computation, 3rd ed., Harper Collins Publishers, New York, NY, pp. 584-596.

14. Flik, M.I., 1991,"Heat Transfer in Superconducting Films", Applied Mechanical Review, Vol. 44, No. 3, March, pp. 93-108.

15. Marezio, M., "Oxygen Stoichiometry in High-T_c Superconductors", 1991, Acta Cryst., A47, p. 646.

16. Cava, R.J. et al., 1990,"Structural Anomalies, Oxygen Ordering and Superconductivity in Oxygen Deficient $Ba_2YCu_3O_x$", Physica C, 165, pp. 419-433.

17. Cava, R.J. et al., 1990,"Structural Anomalies, Oxygen Ordering and Superconductivity in Oxygen Deficient $Ba_2YCu_3O_x$", Physica C, 165, pp. 419-433.

18. Hagen, S.J., Wang, Z.Z. and Ong, N.P., "Anisotrophy of the Thermal Conductivity of $YBa_2Cu_3O_{7-y}$", Physical Review B, 40, 1989, pp. 9389-9392.

19. Touloukian, Y.S. et al. (Eds), 1977, Thermophysical Properties of Matter 13, IFI/Plenum, New York, NY, pp. 158-167.

20. Adachi, H., Hirochi, K., Setsune, K, Kitabatake, M. and Wasa, K., 1987, Applied Physics Letters, 51(26), 28 December, pp. 2263-2265.

21. Runyan, W.R. and Bean, K.E., 1990, Semiconductor integrated Circuit Processing Technology, Addison-Westly Publishing Company, Inc., Reading, MA, pp. 161-293.

22. Shih, I. and Qiu, C.X., 1988,"Chemical Etching of Y-Cu-Ba-O Thin films", Applied Physics Letters, 52(18), May, pp. 1523-1524.

23. Kelkar, M., 1995, "Thermal Boundary Resistance in High Temperature Thin-Film Superconductors", Master's Thesis, University of Hawaii, p. 28.

24. Kelkar, M., 1995, "Thermal Boundary Resistance in High Temperature Thin-Film Superconductors", Master's Thesis, University of Hawaii, p. 29.

25. Phelan, P.E., Song, Y., Nakabeppu, O., Ito, K., Ohmori, T., and Torikoshi, K., 1994, "Film/Substrate Thermal Boundary Resistance For An Er-Ba-Cu-O High-T_c Superconduction Film", Journal of Heat Transfer, Vol. 116, No. 4, pp. 1038-1041.

26. Meyers, G.E., 1987, Analytical Methods in Conduction Heat Transfer, Genium Publishing Corporation, Schenectady, NY, pp. 127-129.

27. Swartz, E.T., 1987, "Solid-State Thermal Boundary Resistance", PhD Thesis, Cornell University, pp. 72-75.

28. Beckwith, T.G., Marangoni, R.D., 1990, Mechanical Measurements, 4th ed., Addison-Wesley Publishing Company, Reading, MA, pp. 43-45.

29. Little, W.A., 1959,"The Transport of Heat Between Dissimilar Solids At Low Temperatures", Canadian Journal of Physics, 37, p. 334.

30. Kelkar, M., Phelan, P.E. and Gu, B.,"Thermal Boundary Resistance for Thin-Film High-T_c Superconductors at Varying Interfacial Temperature Drops", to appear in the International Journal of Heat Transfer.

31. Incropera, F.P. and DeWitt, D.P., 1985, Fundamentals of Heat and Mass Transfer, 2nd ed., John Wiley & Sons, New York, NY, pp. 142-156.

32. Meyers, G.E., 1987, Analytical Methods in Conduction Heat Transfer, Genium Publishing Corporation, Schenectady, NY, p. 313.

33. James, M.L., Smith, G.M., Wolford, J.C., 1985, Applied Numerical Methods for Digital Computation, 3rd ed., Harper Collins Publishers, New York, NY, pp. 584-596.

34. Meyers, G.E., 1987, Analytical Methods in Conduction Heat Transfer, Genium Publishing Corporation, Schenectady, NY, pp. 127-129.

INITIAL DISTRIBUTION LIST

1. Defense Technical Information Center 2
   8725 John J. Kingman Rd., STE 0944
   Ft. Belvoir, VA 22060-6218

2. Dudley Knox Library 2
   Naval Postgraduate School
   411 Dyer Rd.
   Monterey, CA 93943-5002

3. Professor Matthew D. Kelleher, Code ME/MK 1
   Department of Mechanical Engineering
   Naval Postgraduate School
   Monterey, CA 93943-5100

4. Professor Terry R. McNelley, Code ME/TM 1
   Department of Mechanical Engineering
   Naval Postgraduate School
   Monterey, CA 93943-5100

5. Professor Patrick E. Phelan 1
   Arizona State University
   Department of Mechanical and Aerospace Engineering
   PO Box 876106
   Tempe, AZ 85287-6106

6. Naval/Mechanical Curricular Officer 1
   700 Dyer Rd.
   Bldg 245, Rm 115
   Monterey, CA 93943-5109

7. Michael Magee 2
   605 Montecillo Rd.
   San Rafael, CA 94903

8. Dr. Timothy Tong 1
   National Science Foundation
   Chemical and Transport Systems Division
   Thermal Transport and Thermal Processing
   4201 Wilson Blvd.
   Arlington, VA 22230